

THE EVOLUTION OF CLOSED-BASIN BRINES

LAWRENCE A. HARDIE AND HANS P. EUGSTER

Department of Earth and Planetary Sciences, The Johns Hopkins University, Baltimore, Maryland 21218

ABSTRACT

The evolution of closed-basin brines has been investigated with the aid of a model based on evaporative concentration in equilibrium with the atmosphere. Water compositions are restricted to SiO_2 , Ca, Mg, Na, K, HCO_3 , CO_3 , SO_4 and Cl. Evaporation is simulated by a computer program and saturation tests are performed with respect to calcite, sepiolite and gypsum. When saturation occurs, the solids are removed from interaction with the brine. Calculations are terminated at an ionic strength near five.

Sixty-seven subsurface and many closed basin inflow waters have been subjected to the calculations. The calculated brines exhibit the same compositional diversity as the natural brines. However, very few generalizations can be made with respect to brine compositions derived from different rock types. Examination of the detailed mechanisms which determine the eventual fate of a particular water shows that the critical decisions are made very early in the evaporative sequence, at a stage when the calculations are still accurate. Calcite is always the first phase to appear, and it separates carbonate-rich from carbonate-poor brines. The appearance of sepiolite complicates matters and may cause some paths to change direction. Gypsum precipitation also represents a crucial divide.

A flow sheet for brine evolution emerges from the examination of the mechanisms. It relates the four major brine groups to the evolutionary steps. Group a brines ($\text{Na-CO}_3\text{-SO}_4\text{-Cl}$ brines) can be obtained by precipitation of calcite and sepiolite. Group b ($\text{Na}_2\text{SO}_4\text{-NaCl}$) and Group c brines (Na-Mg-Ca-Cl) form by calcite, sepiolite and gypsum precipitation, the choice depending upon the calcium-to-sulfate ratio at the time of gypsum saturation. $\text{Na-Mg-SO}_4\text{-Cl}$ brines (Group d) can only be obtained by retarding sepiolite precipitation, for instance, through using low silica values. Because of the multiple equilibria involved, simple inspection of a water analysis does not reveal its eventual fate upon evaporation.

Calculations are not yet feasible with respect to concentrated brines. Therefore, the fate of concentrated brines has been analyzed by standard graphical procedures based on experimental determinations of brine equilibria. Three Jänecke projections are constructed and they define the last stages of evaporation for any specific brine.

The validity of the model has been tested on several closed basins: Deep Springs, Lake Magadi, Saline Valley, Great Salt Lake and Abert Lake. The correspondence between calculated and natural brine compositions is generally very good. In fact, the model has provided new insights into the hydrology of some of these basins.

The chief limitations of the model are related to the silica removal mechanism, to the artificially fixed Na/K ratio and to the compositional restrictions imposed by the model.

INTRODUCTION

Basins which have no river outlets are common to all continents. Most of them are located in arid or semiarid regions, and many of them receive very considerable quantities of inflow, usually through perennial rivers descending from higher altitudes and disappearing underground before they reach the basin floor. Evaporation on the floor is usually intense, and leads to the deposition of saline minerals. Unlike sea water, the composition of the brines of modern continental evaporites exhibits a bewildering range, lacking any obvious correlation with respect to geography or drainage basin rock types (see Fig. 1). The same diversity is also reflected in the remarkable mineralogy of non-marine evaporites. Yet, like the evaporation of sea water, the evolution of closed basin brines must be governed by a few crucial steps. It is the purpose of this paper to suggest what these steps might be and what controls them.

The compositional history of closed basin waters can be separated into two phases. The first phase deals with the acquisition of solutes by the dilute waters through weathering-type reactions with soil and bedrock. This phase has been discussed by Jones (1966) and by Garrels and Mackenzie (1967), who brilliantly analyzed the case of the Sierra Nevada springs. We shall not comment further on this aspect.

The second phase is concerned with the evaporative concentration which eventually causes the precipitation of very soluble minerals. Jones (1966) and Garrels and

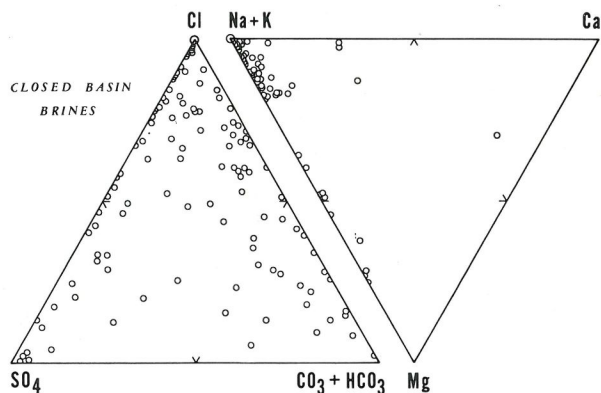


FIG. 1. Compositions of natural closed basin brines in the system $\text{Ca-Mg-Na-K-(HCO}_3\text{+CO}_3\text{)-SO}_4\text{-Cl}$. Sources of analyses: Livingstone (1963), Clarke (1924), Jones (1966), Whitehead & Feth (1961), White *et al.* (1963), Jones (1965), Eugster (1970), Hardie (1968), Talling and Talling (1965). In mole percent.

Mackenzie (1967) have also discussed the critical elements for the understanding of this phase. Garrels and Mackenzie proposed a simple model based on evaporation in equilibrium with the atmosphere and precipitation of minerals such as calcite, sepiolite and gypsum. We have applied their approach with the aid of a computer to many closed-basin waters and to a number of well-documented subsurface waters of igneous, metamorphic and sedimentary environments, taken from the compilation of White *et al.* (1963).

We present the wide variety of evaporation paths and end products produced by these waters. Next, we investigate in detail the mechanisms which define the direction a particular water will follow upon evaporation. From this emerges a general flow sheet for brine evolution, providing for four broad classes of brines. The calculations do not bring us up to saturation with soluble minerals beyond gypsum. To close the gap, we use phase diagrams for each of the four brine classes, from which the final evaporation history for any particular brine can be read quantitatively. We consider the precipitation of trona, mirabilite, thenardite, glauberite, burkeite, bloedite, halite, epsomite, kieserite and bischofite. Finally, the model is tested by applying it to three well-studied basins, Deep Springs, Magadi and Saline Valley.

The model we present here for the evolution of closed-basin brines accounts for many aspects of nonmarine evaporites. We have no illusions, however, with respect to the model's over-simplifications. It can be applied directly to any closed basin, but to account for the finer details, each basin will demand its own particular modification.

CALCULATION OF CHANGES OF WATER COMPOSITION WITH EVAPORATIVE CONCENTRATION

Given the chemical analysis of a dilute natural water, we wish to predict the changes in composition as these waters are progressively evaporated, keeping the partial pressure of CO_2 constant at atmospheric level of $10^{-3.5}$ atm. The basic problem is to take account of the effect precipitation of solids will have on the water composition during evaporative concentration. A solution was provided by Garrels and Mackenzie (1967). We have used their approach as the basis for a computer program that will keep track simultaneously of SiO_2 , Ca, Mg, Na, K, HCO_3^- , CO_3^{2-} , SO_4 , Cl, OH, pH and ionic strength with progressive removal of H_2O . Calcite, sepiolite, amorphous silica and gypsum are the only solid phases possible and no interaction between precipitates and solution is allowed. The method is outlined below.

The variables to be considered are T , P (total), $p\text{CO}_2$, $a\text{H}_2\text{O}$ and the molalities m and activity coefficients γ of the dissolved species. We assume $T = 25^\circ\text{C}$, P (total) = 1 atm., $p\text{CO}_2 = 10^{-3.5}$ atm., and $a\text{H}_2\text{O} = 1$ (the range in natural waters is 1 to about 0.7). To further simplify the calculations, we ignore ion pairing. Thus the only ionic species we consider are Ca^{2+} , Mg^{2+} , Na^+ , K^+ , HCO_3^- , CO_3^{2-} , SO_4^{2-} , Cl^- , OH^- and H^+ and we use the Debye-Hückel equation to calculate activity coefficients. The deviations from real behavior introduced by this assumption will not be appreciable for ionic strengths below about 0.7. As the concentrations get higher the deviations progressively increase but the calculated values are still good "order-of-magnitude" approximations. The choice of solid phases proved a particularly difficult task but we concur with Garrels and Mackenzie that the only likely early precipitates are calcite, sepiolite and gypsum.¹ Also, the calculation procedure does

¹ Dolomite, although a possible precipitate in a closed basin environment, cannot be treated by our method.

not allow SiO_2 to be determined by sepiolite, so we arbitrarily buffered SiO_2 when saturation with amorphous silica had been reached.

The initial step is to recompute a given analysis so that the water is in equilibrium with atmospheric $p\text{CO}_2$. This will obviously affect only the pH dependent species HCO_3^- , CO_3^{2-} and OH^- . The calculation is straightforward. The electrical neutrality equation,

$$2m\text{Ca}^{2+} + 2m\text{Mg}^{2+} + m\text{Na}^+ + m\text{K}^+ + m\text{H}^+ \\ = m\text{HCO}_3^- + 2m\text{CO}_3^{2-} + 2m\text{SO}_4^{2-} + m\text{Cl}^- + m\text{OH}^-$$

is recast so that the only unknowns are pH and the γ_i 's of the pH-dependent species. An iteration process which constantly adjusts pH, I and m and γ for HCO_3^- , CO_3^{2-} and OH^- is used to solve the equation. The details are given in the Appendix. The next step is to test for saturation with the solids calcite, sepiolite and gypsum. For example, if the ion activity product ($a\text{Ca}^{2+} \times a\text{CO}_3^{2-}$) exceeds $10^{-8.34}$ (Garrels and Christ, 1965), then the water is supersaturated with respect to calcite. If saturation with calcite has been reached, then we can set

$$m\text{Ca}^{2+} \cdot \gamma\text{Ca}^{2+} \cdot m\text{CO}_3^{2-} \cdot \gamma\text{CO}_3^{2-} = 10^{-8.34},$$

which allows $m\text{Ca}^{2+}$ to be expressed as a function of pH. We then recast the electrical neutrality equation making $m\text{Ca}^{2+}$ a pH-dependent unknown. In the same way we can make appropriate adjustments to the electrical neutrality equation for saturation with the other solids or assemblages of solids, provided the appropriate ion species can be written in terms of pH and γ_i . In all, equations with pH and γ_i as the only unknowns can be written for the precipitation of calcite alone, sepiolite alone, calcite+sepiolite, calcite+gypsum, and calcite+sepiolite+gypsum (see Appendix).

Evaporation is simulated by doubling all concentrations, until an ionic strength of about 5 is reached, at which time the calculations are terminated.

RESULTS OF THE CALCULATIONS

The results of calculations performed on a number of subsurface waters from the compilation of White *et al.* (1963) are given in Table 1. Figure 2 presents evaporation paths for nine typical waters in terms of the major species. All paths begin at the composition of the natural waters and end at a point of evaporation which produces an ionic strength of about 5. Some general properties of the paths may be noted. As long as calcite alone precipitates, the paths are straight and move away from the Ca and $\text{HCO}_3 + \text{CO}_3$ corners. Precipitation of sepiolite causes curvature in the cation diagram. The waters do not become saturated with respect to gypsum until they are nearly free of $\text{HCO}_3 + \text{CO}_3$. Therefore, all paths in the anion diagram initially move away from the $\text{HCO}_3 + \text{CO}_3$ corner. They move a short distance if the original water contained little alkaline earth, and a long distance if they were rich in Ca and Mg. After nearly all ($\text{HCO}_3 + \text{CO}_3$) has been depleted, they sharply turn away from SO_4 and towards Cl. In most waters, (Ca+Mg) are removed before the Cl corner is reached and the resulting brines are virtually pure (Na+K) brines. Figure 2*i* is an exception, with (HCO_3

TABLE 1. COMPOSITIONS OF DILUTE GROUNDWATERS FROM WHITE *et al.* (1963) AND THE CALCULATED BRINES DERIVED FROM THEM

In mole % of anion sum and cation sum. Crosses indicate phases precipitated: c (calcite), s (sepiolite), g (gypsum). Brine compositions unaffected by low silica are not repeated. Na is for (Na+K), CO₃ is for (HCO₃+CO₃).

| No. | Dilute Waters | | | | | | Brines, Normal Silica | | | | | | | Brines, Low Silica | | | | | | | | | | | |
|-------------------|---------------|------|------|-----------------|-----------------|------|-----------------------|------|------|-----------------|-----------------|------|-----|--------------------|---|----|----|----|-----------------|-----------------|----|---|---|---|--|
| | Ca | Mg | Na | CO ₃ | SO ₄ | Cl | Ca | Mg | Na | CO ₃ | SO ₄ | Cl | c | s | g | Ca | Mg | Na | CO ₃ | SO ₄ | Cl | c | s | g | |
| Igneous Rocks | | | | | | | | | | | | | | | | | | | | | | | | | |
| 1.1 | 25.6 | 9.4 | 65.0 | 73.6 | 6.1 | 20.3 | — | — | 100 | 27.8 | 16.6 | 55.5 | ++- | | | | | | | | | | | | |
| 1.2 | 16.2 | 8.5 | 75.2 | 82.8 | 2.4 | 14.8 | — | — | 100 | 57.0 | 6.0 | 36.9 | +++ | | | | | | | | | | | | |
| 1.4 | 22.0 | 15.0 | 63.0 | 87.2 | 3.9 | 8.7 | — | — | 100 | 57.7 | 13.0 | 29.2 | +++ | | | | | | | | | | | | |
| 1.5 | 6.7 | 1.4 | 91.9 | 71.1 | 7.8 | 21.0 | — | — | 100 | 51.2 | 13.2 | 35.6 | +++ | | | | | | | | | | | | |
| 1.6 | 29.7 | 19.6 | 50.7 | 77.6 | 1.2 | 21.1 | — | — | 100 | 21.6 | 4.1 | 74.3 | +++ | | | | | | | | | | | | |
| 1.7 | 33.9 | 18.5 | 47.6 | 85.3 | 5.2 | 9.5 | — | — | 100 | 32.6 | 24.0 | 43.4 | +++ | | | | | | | | | | | | |
| 1.9 | 48.9 | 18.5 | 32.6 | 76.6 | 17.1 | 6.2 | 0.1 | — | 99.9 | — | 57.5 | 42.4 | +++ | | | | | | | | | | | | |
| 1.10 | 52.9 | 18.7 | 28.4 | 87.6 | 8.4 | 4.0 | 0.1 | — | 99.9 | — | 64.3 | 35.6 | +++ | | | | | | | | | | | | |
| 1.14 | 15.5 | 1.9 | 82.6 | 26.0 | 62.8 | 11.2 | — | — | 100 | — | 82.2 | 17.7 | +++ | | | | | | | | | | | | |
| 2.5 | 16.1 | 81.7 | 2.2 | 94.8 | — | 5.2 | 33.9 | 30.1 | 36.0 | — | — | 100 | +++ | | | | | | | | | | | | |
| 2.6 | 9.2 | 81.8 | 9.0 | 92.4 | 0.6 | 6.8 | 8.6 | 7.7 | 83.6 | — | 0.2 | 99.9 | +++ | | | | | | | | | | | | |
| 2.8 | 30.8 | 35.1 | 34.1 | 84.3 | 3.0 | 12.5 | — | — | 100 | 9.5 | 17.8 | 72.7 | +++ | | | | | | | | | | | | |
| 2.9 | 32.0 | 32.9 | 35.1 | 82.6 | .6 | 16.6 | — | — | 100 | 11.9 | 2.8 | 85.2 | +++ | | | | | | | | | | | | |
| 2.10 | 16.0 | 18.6 | 65.4 | 39.9 | 4.6 | 55.4 | 2.4 | 2.1 | 95.5 | — | 0.4 | 99.6 | +++ | | | | | | | | | | | | |
| 2.12 | 46.9 | 22.6 | 30.5 | 86.9 | 5.0 | 8.0 | — | — | 100 | 6.7 | 35.7 | 57.6 | +++ | | | | | | | | | | | | |
| 2.14 | 40.8 | 30.4 | 28.8 | 77.3 | 5.2 | 17.5 | 0.2 | 0.2 | 99.6 | — | 2.8 | 97.2 | +++ | | | | | | | | | | | | |
| 3.1 | 64.4 | 4.4 | 31.2 | 85.3 | 9.2 | 5.5 | — | — | 100 | — | 57.2 | 42.7 | +++ | | | | | | | | | | | | |
| 3.3 | 72.7 | 6.8 | 20.5 | 56.8 | 37.4 | 5.7 | — | — | 100 | — | 46.9 | 53.0 | +++ | | | | | | | | | | | | |
| 3.4 | 50.6 | 20.2 | 29.2 | 80.2 | 3.8 | 15.8 | — | — | 100 | — | 6.3 | 93.7 | +++ | | | | | | | | | | | | |
| Metamorphic Rocks | | | | | | | | | | | | | | | | | | | | | | | | | |
| 9.1 | 38.0 | 9.6 | 52.4 | 60.1 | 16.4 | 23.2 | — | — | 100 | — | 27.7 | 72.3 | +++ | | | | | | | | | | | | |
| 9.3 | 55.4 | 18.6 | 26.0 | 70.8 | 7.5 | 21.6 | 7.6 | 6.7 | 85.7 | — | .2 | 99.8 | +++ | | | | | | | | | | | | |
| 9.4 | 41.9 | 34.5 | 23.6 | 79.1 | 14.0 | 6.9 | — | — | 100 | — | 38.4 | 61.6 | +++ | | | | | | | | | | | | |
| 9.5 | 55.0 | 31.1 | 13.9 | 77.1 | 19.5 | 3.3 | — | — | 100 | — | 47.0 | 53.0 | +++ | | | | | | | | | | | | |
| 10.1 | 70.6 | 6.4 | 23.0 | 68.4 | 27.4 | 4.1 | — | — | 100 | .1 | 60.8 | 39.1 | +++ | | | | | | | | | | | | |
| 10.2 | 26.6 | 17.0 | 56.4 | 82.1 | 3.1 | 14.7 | — | — | 100 | 37.5 | 10.9 | 51.6 | +++ | | | | | | | | | | | | |
| 10.3 | 43.0 | 11.3 | 45.7 | 84.9 | 3.6 | 11.5 | — | — | 100 | 30.4 | 16.7 | 52.9 | +++ | | | | | | | | | | | | |
| 10.5 | 41.5 | 14.5 | 44.0 | 92.5 | 4.2 | 3.3 | — | — | 100 | 56.4 | 24.3 | 19.2 | +++ | | | | | | | | | | | | |
| 10.6 | 26.4 | 14.6 | 59.0 | 83.5 | 8.4 | 8.0 | — | — | 100 | 41.4 | 29.9 | 28.7 | +++ | | | | | | | | | | | | |
| 10.7 | 71.0 | 12.8 | 16.2 | 81.7 | 14.6 | 3.6 | — | — | 100 | 0.1 | 48.9 | 51.0 | +++ | | | | | | | | | | | | |
| 10.8 | 28.6 | 31.8 | 39.6 | 41.8 | 12.4 | 45.7 | 13.0 | 11.5 | 75.5 | — | .1 | 99.9 | +++ | | | | | | | | | | | | |
| 10.9 | 49.5 | 21.9 | 28.6 | 47.6 | 23.6 | 28.8 | 8.8 | 7.8 | 83.4 | — | .2 | 99.8 | +++ | | | | | | | | | | | | |
| 10.10 | 70.5 | 25.4 | 4.1 | 82.5 | 7.4 | 9.9 | 33.5 | 29.3 | 37.2 | — | .1 | 99.9 | +++ | | | | | | | | | | | | |
| 10.13 | 27.2 | 34.3 | 38.5 | 69.0 | 12.1 | 18.8 | — | — | — | — | 19.9 | 80.1 | +++ | | | | | | | | | | | | |
| Sedimentary Rocks | | | | | | | | | | | | | | | | | | | | | | | | | |
| 4.3 | 31.1 | 20.5 | 48.4 | 88.8 | 8.2 | 2.9 | — | — | 100 | 43.5 | 41.9 | 14.6 | +++ | | | | | | | | | | | | |
| 4.4 | 55.9 | 34.1 | 10.0 | 65.9 | 16.6 | 17.5 | 25.4 | 22.5 | 52.1 | — | .1 | 99.9 | +++ | | | | | | | | | | | | |
| 4.5 | 74.5 | 14.7 | 10.8 | 95.6 | 0.7 | 3.6 | — | — | 100 | 10.4 | 14.8 | 74.7 | +++ | | | | | | | | | | | | |
| 4.6 | 54.0 | 15.4 | 30.6 | 84.4 | 9.5 | 6.1 | — | — | 100 | 0.1 | 53.4 | 46.5 | +++ | | | | | | | | | | | | |
| 4.8 | 50.2 | 21.5 | 28.3 | 89.9 | 2.0 | 8.1 | — | — | 100 | 22.1 | 15.5 | 62.4 | +++ | | | | | | | | | | | | |
| 4.11 | 44.2 | 19.7 | 36.1 | 94.6 | 4.4 | 1.0 | — | — | 100 | 59.5 | 33.2 | 7.3 | +++ | | | | | | | | | | | | |
| 4.13 | 37.0 | 39.9 | 23.1 | 92.0 | 7.7 | 0.2 | — | — | 100 | 0.1 | 96.7 | 3.2 | +++ | | | | | | | | | | | | |
| 5.1 | 18.4 | 12.7 | 68.9 | 63.5 | 2.5 | 34.0 | — | — | 100 | 18.1 | 5.6 | 76.2 | +++ | | | | | | | | | | | | |
| 5.2 | 16.0 | 13.2 | 70.8 | 2.7 | 78.9 | 18.4 | — | — | 100 | — | 68.4 | 31.5 | +++ | | | | | | | | | | | | |
| 5.4 | 26.5 | 16.6 | 56.9 | 82.5 | 9.9 | 7.5 | — | — | 100 | 35.2 | 36.9 | 27.9 | +++ | | | | | | | | | | | | |
| 5.5 | 59.9 | 19.5 | 20.6 | 43.0 | 43.7 | 13.3 | — | — | 100 | — | 11.0 | 88.9 | +++ | | | | | | | | | | | | |
| 5.8 | 15.0 | 5.2 | 79.8 | 69.2 | 10.2 | 20.5 | — | — | 100 | 38.0 | 20.7 | 41.3 | +++ | | | | | | | | | | | | |
| 5.11 | 76.0 | 16.0 | 7.0 | 47.1 | 48.1 | 4.6 | — | — | 100 | — | 14.8 | 85.1 | +++ | | | | | | | | | | | | |
| 5.12 | 34.6 | 32.4 | 33.0 | 72.6 | 26.4 | 0.9 | — | — | 100 | — | 93.4 | 6.5 | +++ | | | | | | | | | | | | |
| 5.13 | 1.5 | 0.1 | 98.4 | 68.6 | 0.2 | 31.1 | — | — | 100 | 54.8 | 0.2 | 45.0 | +++ | | | | | | | | | | | | |
| 5.14 | 5.4 | 5.4 | 89.2 | 36.8 | .1 | 63.1 | — | — | 100 | 15.0 | .1 | 84.9 | +++ | | | | | | | | | | | | |
| 5.15 | 0.6 | 0.3 | 99.1 | 35.6 | .1 | 64.2 | — | — | 100 | 23.9 | .1 | 76.0 | +++ | | | | | | | | | | | | |
| 5.16 | 32.1 | 18.2 | 49.7 | 6.4 | 86.9 | 6.7 | — | — | 100 | 0.1 | 80.5 | 19.4 | +++ | | | | | | | | | | | | |
| 5.18 | 28.6 | 21.6 | 49.8 | 1.5 | 75.2 | 23.2 | — | — | 100 | — | 40.6 | 59.3 | +++ | | | | | | | | | | | | |
| 6.2 | 89.0 | 4.1 | 6.9 | 94.9 | 1.5 | 3.5 | 0.4 | 0.4 | 99.2 | — | 3.4 | 96.6 | +++ | | | | | | | | | | | | |
| 6.3 | 73.6 | 14.7 | 11.7 | 91.2 | 2.3 | 6.5 | .6 | .5 | 98.9 | — | 1.9 | 98.1 | +++ | | | | | | | | | | | | |
| 6.5 | 49.9 | 31.6 | 18.4 | 90.9 | 0.5 | 8.5 | — | — | 100 | 5.6 | 5.7 | 88.7 | +++ | | | | | | | | | | | | |
| 6.6 | 58.3 | 34.5 | 7.2 | 81.7 | 17.4 | 0.9 | — | — | 100 | — | 68.0 | 31.9 | +++ | | | | | | | | | | | | |
| 6.7 | 86.8 | 2.4 | 10.8 | 94.5 | 0.1 | 5.2 | — | — | 100 | 5.7 | .9 | 93.3 | +++ | | | | | | | | | | | | |
| 6.8 | 53.4 | 11.3 | 35.3 | 82.0 | 3.7 | 14.2 | — | — | 100 | 4.7 | 19.9 | 75.4 | +++ | | | | | | | | | | | | |
| 6.11 | 54.7 | 36.2 | 9.1 | 57.7 | 39.3 | 3.0 | — | — | 100 | — | 38.7 | 61.3 | +++ | | | | | | | | | | | | |
| 6.12 | 62.7 | 23.4 | 13.9 | 86.9 | 7.4 | 5.6 | — | — | 100 | — | 20.7 | 79.3 | +++ | | | | | | | | | | | | |
| 6.14 | 53.2 | 25.7 | 21.1 | 44.6 | 39.5 | 15.8 | .4 | .4 | 99.2 | — | | | | | | | | | | | | | | | |

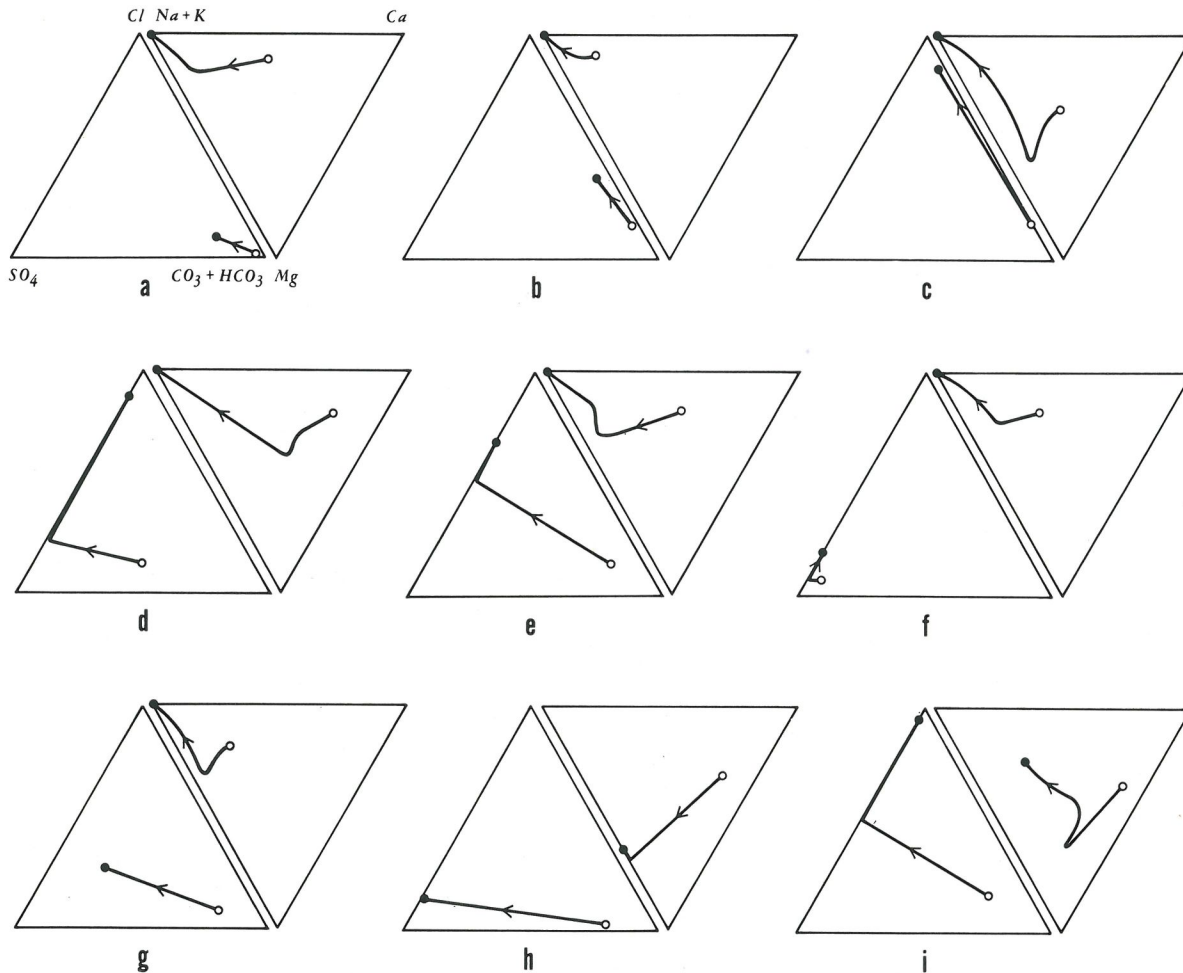


FIG. 2. Individual calculated evaporation paths. Open circles are dilute waters and solid circles are brines at an ionic strength of 5. a: Sierra Nevada Springs (Feth *et al.*, 1964, and Garrels and Mackenzie, 1967); b: rhyolite water W 1.2; c: basalt water W 2.9; d: shale water W 5.5; e: average North American river water (Livingstone, 1963); f: shale water W 5.16; g: Deep Springs Lake, California, Bog-Mound Spring (Jones, 1965); h: quartzite water W 9.5; i: sandstone water W 4.4 (all W waters from White *et al.*, 1963). In mole percent.

cause of the high alkaline earth content, leads to a chloride brine. Limestone waters (*e.g.* W 6.5) may produce a very similar path.

In all three cases (a, b and c) gypsum saturation is never reached, because either initial SO_4 or initial Ca are too low. The brines produced, therefore, are carbonate-chloride brines. Paths for sulfate-rich waters are shown in Figure 2d, e and f. Waters d and f are from shales and e is average North American river water (Livingstone, 1963); d produces a chloride brine through precipitation of large amounts of gypsum. The average river water contains less sulfate, but the calcium is exhausted earlier, producing a sulfo-chloride brine. The Pierre shale water (f) is very unusual because of its exceedingly high sulfate content; its Ca is precipitated quickly and it remains a sodium sulfate brine.

The water of Figure 2g is from a spring in Deep Springs Valley (Jones, 1965), and it produces a mixed brine, while

path h has been obtained from a water of a metamorphic terrane by retarding sepiolite precipitation through a low silica input. The latter ends up as a Na-Mg sulfate brine. Path i, based on a water from sandstone, is unusual. It starts with a low Na content and exhausts its $(\text{HCO}_3 + \text{CO}_3)$ and SO_4 , producing a Ca-Mg-Na-Cl brine.

Actual brines corresponding to the nine examples chosen for Figure 2 are Alkali Valley, Oregon, and Lake Magadi, Kenya, for a and b; Abert Lake, Oregon, for c; Great Salt Lake, Utah, for d; Saline Valley, California for e; Devils Lake, North Dakota for f; Deep Springs Lake, California for g; Poison Lake, Washington for h and Bristol Lake, California for i.

Figure 3 compares the compositions of 63 initial waters with those of the brines they produce. Inflow waters (Fig. 3a), as is well known, are predominantly of the Na-Ca-bicarbonate type. During evaporation the points, which were initially clustered mainly around the $(\text{HCO}_3 + \text{CO}_3)$

corner, scatter throughout the anionic diagram with some concentration around the Cl corner and the Cl-SO₄ side (Fig. 3b). Conversely, the initial scatter in the cationic diagram is greatly reduced, because the vast majority of brines end up in the Na corner (Fig. 3b). Comparing the natural (Fig. 1) with the synthetic (Fig. 3b) brine compositions is a good test of the applicability of the model. Even for such biased sample populations the correspondence is excellent, except with respect to the MgSO₄-rich brines. This remaining discrepancy will be clarified later. The general evolution of water compositions emerging from Figure 3 is the trend proposed by Hutchinson (1957), and discussed by Jones (1966).

We may conclude then, that the observed compositional diversity of natural brines can be accounted for entirely by the differences in inflow water compositions, coupled with evaporative concentration and precipitation of calcite, a hydroxy silicate such as sepiolite, and gypsum.

The data contained in Table 1 and Figure 3 throw light on another important question, the relation between final brine composition and rock type from which the initial water derived its solutes. As Figure 3 clearly demonstrates, few safe generalizations can be made. Identical brines can

result from waters of very different rock types, e.g. basalt W 2.9 (Fig. 2c) and limestone W 6.5 (Table 1).

INTERPRETATION OF THE EVAPORATION PATHS: THE CRITICAL MECHANISMS

For all waters we processed through the computer program calcite was found to be the first precipitate, generally at ionic strengths considerably less than 0.01. Throughout progressive evaporation of a water which is continuously precipitating calcite, the following restrictions must hold:

1. Ca²⁺ and CO₃²⁻ must be lost from solution in equal molar proportions, and
2. the IAP ($a_{Ca^{2+}} \cdot a_{CO_3^{2-}}$) of the solution must remain constant at constant P (total) and T .

Now, because the initial molar proportions in general will not be equal, the first restriction implies that the Ca²⁺ to CO₃²⁻ proportions in the solution must change as calcite precipitates. The second restriction allows only antipathetic changes in Ca²⁺ and CO₃²⁻ concentrations, that is, if Ca²⁺ increases then CO₃²⁻ must decrease, and *vice versa*. Clearly, then, early calcite precipitation is a critical evolutionary step: it will immediately determine whether an evaporating water will become carbonate-rich or carbonate-poor.

To understand just how this step determines the actual evaporation paths, it is easiest to first take a simple case. Consider the system Ca-CO₂-H₂O at 25°C, 1 atm total pressure and $pCO_2 = 10^{-3.5}$. Let us assume ideal solution and that $a_{H_2O} = 1$. If the only dissolved ionic species are Ca²⁺, H⁺, CO₃²⁻, HCO₃⁻, OH⁻ then by electrical neutrality we have

$$2mCa^{2+} + mH^+ = 2mCO_3^{2-} + mHCO_3^- + mOH^-$$

Using the well established equilibria in the system H₂O-CO₂ (Garrels and Christ, 1965, p. 76), we can express H⁺, HCO₃⁻ and OH⁻ in terms of CO₃²⁻, as follows:

$$mH^+ = 10^{-10.825}(mCO_3^{2-})^{-1/2}$$

$$mHCO_3^- = 10^{-0.495}(mCO_3^{2-})^{1/2}$$

$$mOH^- = 10^{-3.175}(mCO_3^{2-})^{1/2}$$

Substituting in the electrical balance equation, and neglecting mH^+ gives

$$mCa^{2+} = mCO_3^{2-} + 10^{-0.795}(mCO_3^{2-})^{1/2} \quad (1)$$

This equation (1) gives the calcium-carbonate concentration relations on evaporation of the solution. It is plotted as the solid curve in Figure 4. At equilibrium with calcite the system becomes invariant because of the additional restriction $mCa^{2+} \cdot mCO_3^{2-} = 10^{-8.34}$, and hence continued precipitation of calcite will not change the calcium-carbonate concentrations. Now, if other ionic species such as Na⁺, K⁺, Mg²⁺, Cl⁻, SO₄²⁻ are added to the system, equation (1) becomes

$$mCa^{2+} = mCO_3^{2-} + 10^{-0.795}(mCO_3^{2-})^{1/2} + \Delta \quad (1')$$

where

$$\Delta = 1/2\{mCl^- + 2mSO_4^{2-}\} - (mNa^+ + mK^+ + 2mMg^{2+})\}$$

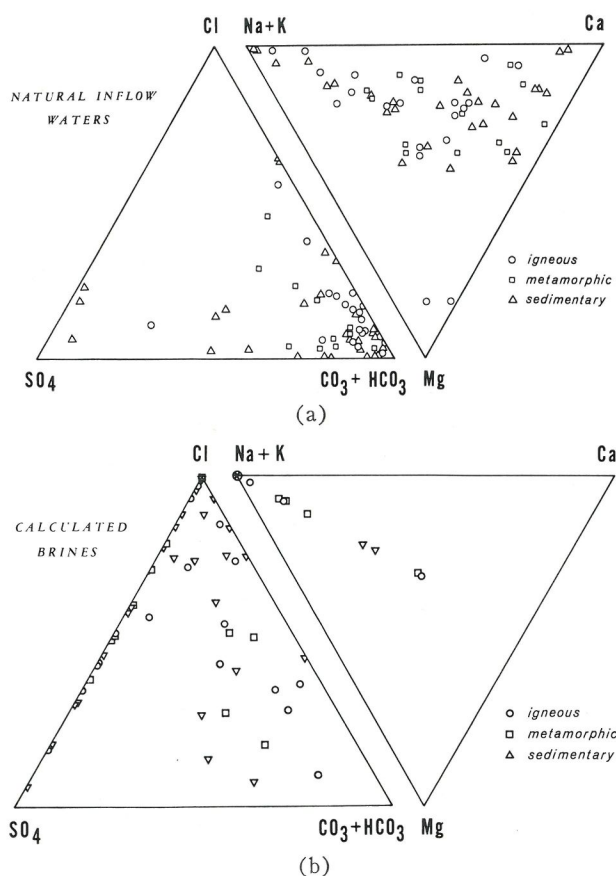


FIG. 3. Composition of dilute groundwaters (Fig. 3a) and the calculated brines (Fig. 3b) produced from them for the analyses of Table 1. In mole percent.

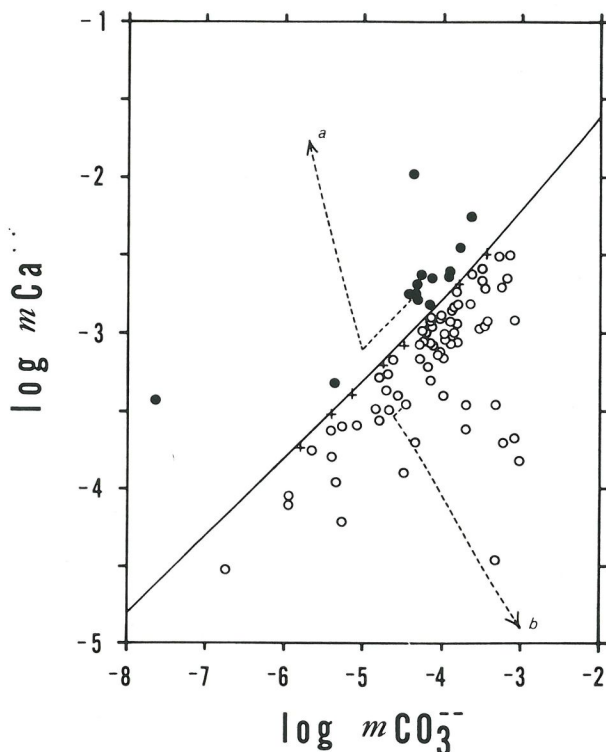


FIG. 4. Calcium-carbonate concentrations (\log_{10} molality) of natural groundwaters and inflow waters recalculated to equilibrium with atmospheric P_{CO_2} . Open circles are waters which become carbonate-rich and calcium-poor with continued calcite precipitation on evaporation (curve *b* is a typical evaporation path); solid circles are waters which do just the opposite (typical path is curve *a*). Crosses are waters which show little change in either calcium or carbonate. The solid curve is for the simple, ideal system $\text{Ca-CO}_2\text{-H}_2\text{O}$ at 25°C , $P(\text{total})=1$ atm. and $P_{\text{CO}_2}=10^{-3.5}$ (equation 1 in the text).

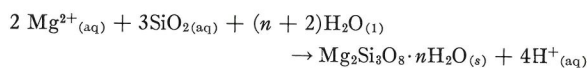
The effect is to move the curve in Figure 4 to the calcium side for a positive Δ and to the carbonate side for a negative Δ without changing the slope. At equilibrium with calcite this more complex system is not invariant, the value of Δ is free to change and hence the values of $m\text{Ca}^{2+}$ and $m\text{CO}_3^{2-}$ will also change. However, these changes can only be such that the product $m\text{Ca}^{2+} \cdot m\text{CO}_3^{2-}$ remains constant at $10^{-8.34}$, hence,

$$10^{-8.34} = m\text{CO}_3^{2-} \{ (m\text{CO}_3^{2-}) + 10^{0.795}(m\text{CO}_3^{2-})^{1/2} + \Delta \} \quad (2)$$

As evaporation proceeds, the absolute value of delta, (Δ), increases so that a solution with an initially negative Δ (calcium "deficient") must markedly and progressively increase in $m\text{CO}_3^{2-}$ at the expense of $m\text{Ca}^{2+}$. A solution with a positive Δ must show just the reverse. A solution with a zero Δ will, of course, show no change in either $m\text{CO}_3^{2-}$ or $m\text{Ca}^{2+}$ on evaporation. The principle also holds for real solutions in which $a_i \neq m_i$. This is illustrated in Figure 4, which is a plot of the initial values of $m\text{Ca}^{2+}$ against $m\text{CO}_3^{2-}$ of 94 natural waters equilibrated with atmospheric $p\text{CO}_2$. Quantitative evaporation paths were

calculated for each water, allowing calcite as the only precipitate. Open circles are those waters which became CO_3^{2-} -enriched and solid circles are waters which ended Ca^{2+} rich. Typical paths are shown as the dashed curves *a* and *b*. As the diagram shows, the ideal simple system evaporation curve divides the two opposing trends, as would be predicted for real solutions dilute enough that activity coefficient corrections are quite small. Waters which show only relatively little change in $m\text{CO}_3^{2-}/m\text{Ca}^{2+}$ on evaporation are plotted as crosses. These waters fall on or close to the simple system path. Since they correspond to zero or small Δ solutions, their $m\text{CO}_3^{2-}/m\text{Ca}^{2+}$ ratio should not change on evaporation. However, at higher concentrations the activity coefficients add significant corrections so that the ratio does, in fact, progressively increase, although no great deviations occur. These waters never become enriched in either calcium or carbonate.

The distribution of points in Figure 4 indicates that most natural waters should end up as carbonate-enriched brines. This is in marked contrast to the natural situation where less than half the closed basin brines are carbonate-rich (see Fig. 1). The key to this anomaly is found in the profound influence precipitation of sepiolite has on the evaporation paths. For more than half the waters in the carbonate field of Figure 4 sepiolite precipitation following after calcite causes a complete reversal in the initial carbonate enrichment trend. A typical path taken by one of these waters is shown in Figure 5. The critical factor is the release of hydrogen ions by the sepiolite precipitation reaction *i.e.*,



If hydrogen ion concentration increases with continued sepiolite precipitation, then the CO_3^{2-} concentration must decrease, because at a fixed $p\text{CO}_2$ of $10^{-3.5}$ the relation $[\text{CO}_3^{2-}][\text{H}^+]^2 = 10^{-21.65}$ holds. Whether a given water will show an increase or a decrease in $m\text{CO}_3^{2-}$ as sepiolite co-precipitates with calcite depends primarily upon the $m\text{Ca}^{2+} + m\text{Mg}^{2+}/m\text{CO}_3^{2-}$ ratio at the point of initial saturation with sepiolite. This is best demonstrated by the same kinds of arguments used above for calcite. The alkaline earth-carbonate relations in an ideal solution are given by

$$m\text{Ca}^{2+} + m\text{Mg}^{2+} = m\text{CO}_3^{2-} + 10^{-0.795}(m\text{CO}_3^{2-})^{1/2} + \Delta \quad (3)$$

where

$$\Delta = 1/2 \{ (m\text{Cl}^- + 2m\text{SO}_4^{2-}) - (m\text{Na}^+ + m\text{K}^+) \}$$

In Figure 6 the relations given by equation (3) for $\Delta=0$ are plotted as the solid curve. This curve defines the boundary between the $+\Delta$ and $-\Delta$ fields. The values of $(m\text{Ca}^{2+} + m\text{Mg}^{2+})$ and $m\text{CO}_3^{2-}$ were calculated for 61 natural waters at the point of first co-precipitation of sepiolite + calcite. They are plotted in Figure 6 as solid circles for those waters which showed a carbonate decrease, and as open circles for those that showed a carbonate increase, on continued co-precipitation of sepiolite + calcite. Typical evaporation paths for these two opposing trends are shown as the dashed curves *a* and *b*. The solid curve, although

rigorously valid only for ideal waters, does divide the fields of the natural waters and so provides a good graphical demonstration of the critical evolutionary parameter $mCa^{2+} + mMg^{2+}/mCO_3^{2-}$. The agreement is good because at the point of first precipitation of sepiolite the waters are still dilute: for all the waters considered sepiolite saturation was reached at ionic strengths less than 0.1. Waters having $\Delta \cong 0$ should, on evaporation, show no changes in alkaline earth or carbonate concentration except those imposed by deviation from nonideal behavior.

The significant conclusion is that the major compositional trend a water will follow is determined *at a very early stage in the evaporation history* by calcite precipitation or coprecipitation of calcite+sepiolite. Waters following the carbonate enrichment trend rapidly lose their alkaline earths so that the next precipitation step occurs only at the high concentrations required for saturation with the very soluble alkali salts. On the other hand, waters that follow the alkaline earth enrichment trend soon reach saturation with the moderately soluble gypsum. When this occurs another critical step in their evolution is met. This step will determine whether the water will ultimately become calcium rich and sulfate poor or just the reverse. The principle involved is the same as we outlined for calcite. During precipitation of gypsum Ca^{2+} and SO_4^{2-} are removed from the evaporating brine in equal molar proportions but the ion activity product $aCa^{2+} \cdot aSO_4^{2-}$ must remain constant. Ionic strengths at gypsum saturation range from 0.1 to 0.7 so that the activity coefficients deviate significantly from one. Therefore the Ca^{2+}/SO_4^{2-} dividing line which separates calcium enrichment from sulfate enrichment cannot

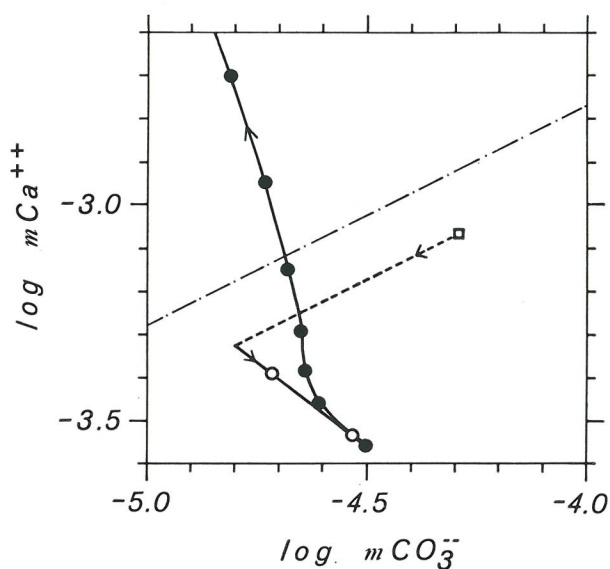


FIG. 5. A typical evaporation path for a water that reverses direction on precipitation of sepiolite. Square is initial composition (in this case supersaturated with respect to calcite); curve through open circles is calcite precipitation path; curve through solid circles is calcite+sepiolite precipitation path. Dot-dash curve is equation (1).

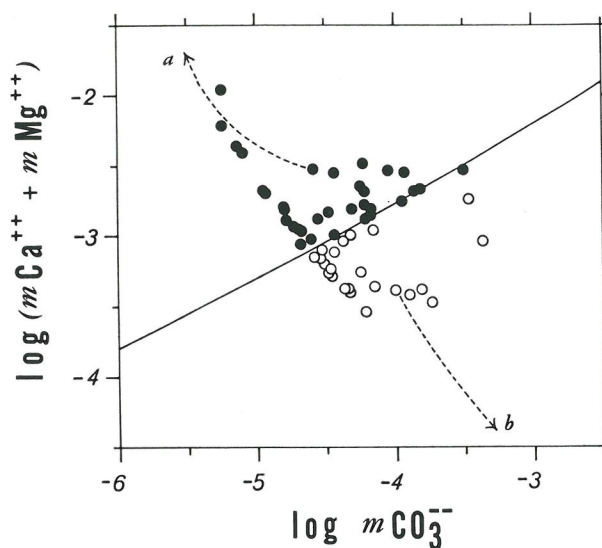


FIG. 6. Calculated alkaline earth-carbonate concentrations (\log_{10} molality) of natural groundwaters at the point of initial co-precipitation of calcite+sepiolite. Open circles are waters which become carbonate-rich and alkaline earth-poor on evaporative concentration (curve b is a typical path); solid circles are waters which do just the opposite (curve a is a typical path). The solid curve is for the alkaline earth-carbonate relations in the simple, ideal system $Ca-Mg-CO_2-H_2O$ (equation 3 for $\Delta=0$).

be safely predicted by simple inspection, as was possible for calcite precipitation, (e.g. Fig. 4).

A FLOW SHEET FOR BRINE EVOLUTION

The analysis of the critical mechanisms leads immediately to a simple flow sheet, Figure 7, for an evaporating spring, well or river water. As a dilute water is concentrated, it quickly reaches saturation with calcite. At this point, very early in its history, it may increase in carbonate + bicarbonate and decrease in calcium (Path I in Fig. 7) or it may do just the opposite (Path II in Fig. 7). If waters

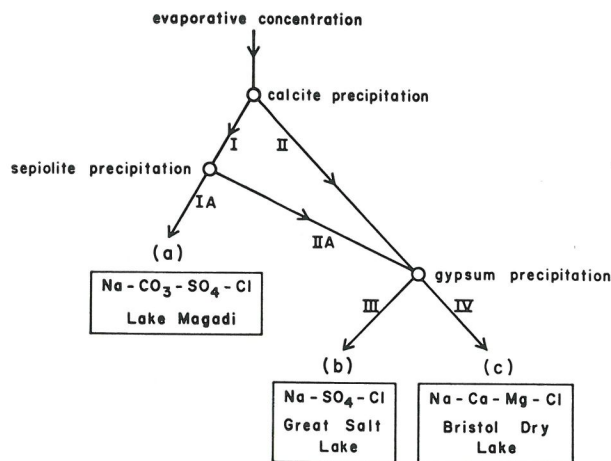


FIG. 7. A flow sheet for evaporative concentration of dilute waters assuming reported silica concentrations.

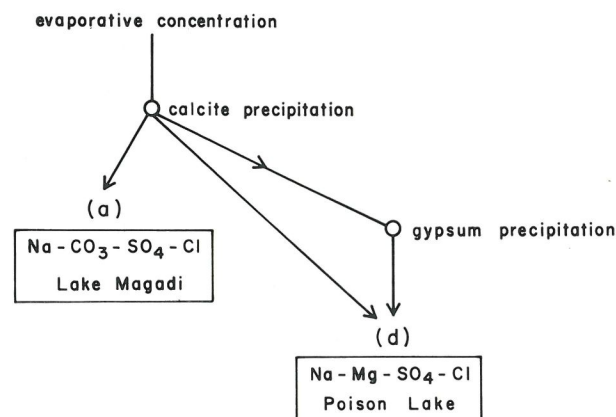


Fig. 8. A flow sheet for evaporative concentration of dilute waters assuming an initial silica concentration of 0.0001 ppm.

that follow Path I reach sepiolite saturation then a second choice is presented: they can become carbonate-enriched and alkaline earth-poor (Path IA) or *vice versa* (Path IIA). (The factors which determine the precise dividing points for a particular water have been discussed above). Path I-IA leads to $\text{Na}-\text{CO}_3-\text{SO}_4-\text{Cl}$ brines (Group a) typified by the waters of Lake Magadi, Kenya; Deep Springs Lake, California etc. If the waters follow paths II or IIA they ultimately precipitate gypsum and may become sulfate rich and calcium poor (Path III) or *vice versa* (Path IV).¹ Path III produces $\text{Na}-\text{SO}_4-\text{Cl}$ brines (Group b) like those of Great Salt Lake, Utah; Saline Valley, Calif. etc. Waters following Path IV become depleted in sulfate and end as $\text{Na}-\text{Ca}-\text{Mg}-\text{Cl}$ brines (Group c) such as those of Bristol Dry Lake and Cadiz Lakes of California. The final fate of these three major types of brines is treated below.

The fourth major naturally occurring brine type is the $\text{Mg}-\text{Na}-\text{SO}_4-\text{Cl}$ group, typified by the high magnesium sulfate waters of Little Manitou Lake, Saskatchewan and Poison Lake, Washington. Brines of these compositions (Group d brines) cannot be reached by our computer program in its present form because we had to buffer SiO_2 by amorphous silica and, therefore, magnesium had to always decrease with sepiolite precipitation. Although an obviously unreal situation it does produce the low silica-low magnesium concentrations common to most natural brines. High magnesium values can be produced by failure to nucleate sepiolite. However, if this alone were the case, then simple evaporative concentration of the normal silica of natural waters would produce unacceptably high silica concentrations, way in excess of any found in natural brines (Jones *et al.*, 1967). The problem centers upon the removal of silica at a very early stage in the evaporation history (by some mechanism unknown, perhaps the conversion of kaolin to montmorillonite or sorption on stable clays,

¹ Sepiolite precipitation does not change the evolutionary path of path II waters and so has not been included in the flow sheet.

Jones and Berner, pers. commun.). If this is the case, then sepiolite saturation will not be reached until magnesium concentrations are already high. We have reproduced this situation artificially in our calculations by starting with an arbitrary, low silica input (0.0001 ppm). From the evaporation paths so calculated for 63 natural waters (see Table I) we have constructed the flow sheet given in Figure 8. The diagram does show two paths by which $\text{Mg}-\text{Na}-\text{SO}_4-\text{Cl}$ brines might indeed be reached. An example of a complete path of this sort is shown in Figure 2h.

FATE OF THE CONCENTRATED BRINES

The calculations were terminated at an ionic strength of about 5. However, there is a very considerable body of data available on the phase relations of the more soluble salts which would precipitate upon continuing evaporation. These data can most easily be built into our model through the normal graphical procedures. For this purpose we can use as a basis the four brine groups developed in Figures 7 and 8.

(a) $\text{Na}-\text{CO}_3-\text{SO}_4-\text{Cl}$ brines

Brines of this type have been discussed by Jones (1965) and by Eugster (1970), and are exemplified by Deep Springs Lake, California and Lake Magadi, Kenya. Of the 63 brines in Table 1, 27 fall into this class. They can be plotted in an anion diagram $\text{SO}_4-\text{CO}_3-\text{Cl}$ and their phase relations can be treated in the system $\text{NaHCO}_3-\text{Na}_2\text{CO}_3-\text{Na}_2\text{SO}_4-\text{NaCl}$. Jones (1965) has presented a diagram at 20°C, based on Teeple's (1929) data, in which P_{CO_2} is allowed to vary. Since P_{CO_2} is fixed in our calculations, we can construct a section at atmospheric P_{CO_2} through this system using the data of Teeple (1929) Makarov and Blidden (1938), D'Ans (1933), Eugster (1965) and Bradley and Eugster (1969). Data are available for 20, 35 and 50°C. Figure 9 gives the phase boundaries for 20°C, which is probably closest to average evaporating temperatures. Primary crystallization fields are shown for mirabilite-thenardite, trona, halite and burkeite. The size of the burkeite field is very sensitive to P_{CO_2} and T , and it expands considerably with increases in these two parameters. The synthetic brines derived by computer evaporation to $I \sim 5$ (Table 1) have been plotted in this diagram as open circles. From here it is easy to predict crystallization sequences, based on the normal rules for a ternary diagram applied to this Jänecke-type projection. The bulk of the brines lie to the right of the line bh and will, upon complete evaporation, yield the assemblage trona + burkeite + halite with the last brine at E; all other brines will stop at the peritectic P .

(b) $\text{NaCl}-\text{Na}_2\text{SO}_4$ brines

Hardie (1968) has discussed brines of this type from the Saline Valley, California, deposit. By the time the computer evaporation end point is reached, little calcium remains in the brines, and the only phases which can precipitate upon further evaporation are halite and thenardite. Glauberite ($\text{Na}_2\text{SO}_4 \cdot \text{CaSO}_4$) is an earlier precipitate or reaction product, and it has not been taken into account in

the calculations. To include it we must consider the brine compositions at the moment of gypsum saturation.

Figure 10 shows the Jänecke projection of the system $\text{CaSO}_4\text{—Na}_2\text{SO}_4\text{—NaCl—H}_2\text{O}$ at 25°C , recalculated from Hardie (1968) and based on the compilation of D'Ans (1933). Gypsum dominates the diagram and crowds all phase boundaries to the $\text{NaCl—Na}_2\text{SO}_4$ side. As the schematic insert shows, glauberite occupies in this diagram a position similar to that of burkeite in Figure 9. All brines to the right of the line $gl\text{—}h$ terminate at *E*, with the initially precipitated gypsum replaced by glauberite through reaction with the brine. All other brines terminate at *P*.

Of the 63 brines of Table 1, 28 fall into group b. Their compositions have been plotted in Figure 10 at initiation of gypsum precipitation. They are scattered throughout the diagram with about an equal number producing gypsum + glauberite + halite (point *P*) and glauberite + thenardite + halite assemblages (point *E*).

With the aid of Figure 10 it is possible to include the presence of glauberite and to derive for any particular water the sequence of events to be expected upon further evaporation.

(c) Na—Mg—Ca—Cl brines

Minerals in this system are halite (NaCl), bischofite ($\text{MgCl}_2 \cdot 6\text{H}_2\text{O}$), antarcticite ($\text{CaCl}_2 \cdot 6\text{H}_2\text{O}$) and tachyhydrite ($\text{CaMg}_2\text{Cl}_6 \cdot 12\text{H}_2\text{O}$). Equilibrium data on the system $\text{NaCl—MgCl}_2\text{—CaCl}_2\text{—H}_2\text{O}$ are scarce. Moreover, they are not directly applicable to the natural chloride brines, which always contain KCl . We therefore should also consider the minerals sylvite (KCl), carnallite ($\text{KMgCl}_3 \cdot 6\text{H}_2\text{O}$) and chlorocalcite (KCaCl_3). However, our program artificially fixes the Na/K ratio throughout, so that the alkali ratio of the calculated brines is meaningless. A comparison between natural and calculated brines in this group is not useful until the behaviour of the alkalis during evaporative concentration is better known and the computer program has been adjusted accordingly.

(d) $\text{Na—Mg—SO}_4\text{—Cl}$ brines

According to the flow sheets (see Figs. 7 and 8), all waters which produced Group b and c brines in the high silica case will produce Group d brines for the case of low silica content. The fate of Group d brines upon further evaporation can be explored conveniently in the reciprocal system $\text{Na}_2\text{Cl}_2\text{—Na}_2\text{SO}_4\text{—MgCl}_2\text{—MgSO}_4$. D'Ans (1933) and Autenrieth and Braune (1960) have summarized the relevant data for this system and Figure 11 shows the 25°C isotherm in a Jänecke projection. For the sake of simplicity, field boundaries are drawn as straight lines. The field is dominated by bloedite ($\text{Na}_2\text{SO}_4 \cdot \text{MgSO}_4 \cdot 4\text{H}_2\text{O}$) and epsomite ($\text{MgSO}_4 \cdot 7\text{H}_2\text{O}$), in addition to halite, thenardite and mirabilite. Very close to the MgCl_2 corner there are small fields for hexahydrite ($\text{MgSO}_4 \cdot 6\text{H}_2\text{O}$), kieserite ($\text{MgSO}_4 \cdot \text{H}_2\text{O}$) and bischofite ($\text{MgCl}_2 \cdot 6\text{H}_2\text{O}$). Crystallization proceeds towards the MgCl_2 corner, with the most concentrated brines at the bischofite + kieserite + halite + solution point. All starting compositions in the halite—bloedite—thenardite triangle terminate at point *A*,

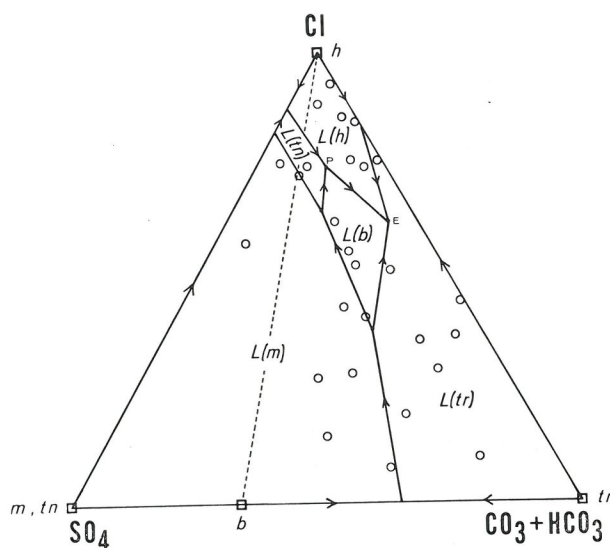


FIG. 9. Phase relations and compositions of calculated brines (Table 1) in the system $(\text{HCO}_3 + \text{CO}_3)\text{—SO}_4\text{—Cl}$. Cation is Na . Phase boundaries for 20°C , $P_{\text{CO}_2} = 10^{-3.5}$ atm. For source of data, see text. tr: trona, m: mirabilite, tn: thenardite, b: burkeite, h: halite. *L(s)* represents the composition of a brine saturated with respect to the solid *s*. Arrows are isothermal evaporation paths, drawn as straight lines for simplicity. *P* is a reaction point ("peritectic") and *E* is the most concentrated brine ("eutectic"). In mole percent. Brines plotted at ionic strengths of 5.

outside of the triangle because of the incongruent solubility of bloedite; all starting compositions in the halite—bloedite—epsomite triangle terminate at point *B*, and the remaining ones at point *C*.

All 37 brines which fall into this group have been plotted in Figure 11. They are scattered throughout the diagram, but the majority of them will yield epsomite + bloedite + halite assemblages.

The most surprising result of Figure 11 is the size of the bloedite field; 16 of the plotted brines should produce bloedite as the first precipitate after calcite, sepiolite and gypsum, and in all other cases but one, it occurs as the second saline mineral. Bloedite has been reported from very few Na—Mg sulfate lakes in North America, but it is possible that it has been overlooked in a number of deposits.

APPLICATION TO CLOSED BASINS

Up to now we have discussed and calculated the fate of a number of dilute river and spring waters upon simulated evaporation and have shown that our simple model can account for the diversity of natural closed basin brine compositions (Fig. 1). The crucial test of the model, however, is the detailed comparison with natural brines of specific closed basins. The necessary information is available for a number of basins, among them Deep Springs Lake (Jones, 1965), Saline Valley (Hardie, 1968), Abert Lake (Jones, 1966), Great Salt Lake (Hahl and Langford, 1964) and Lake Magadi (Eugster, 1970).

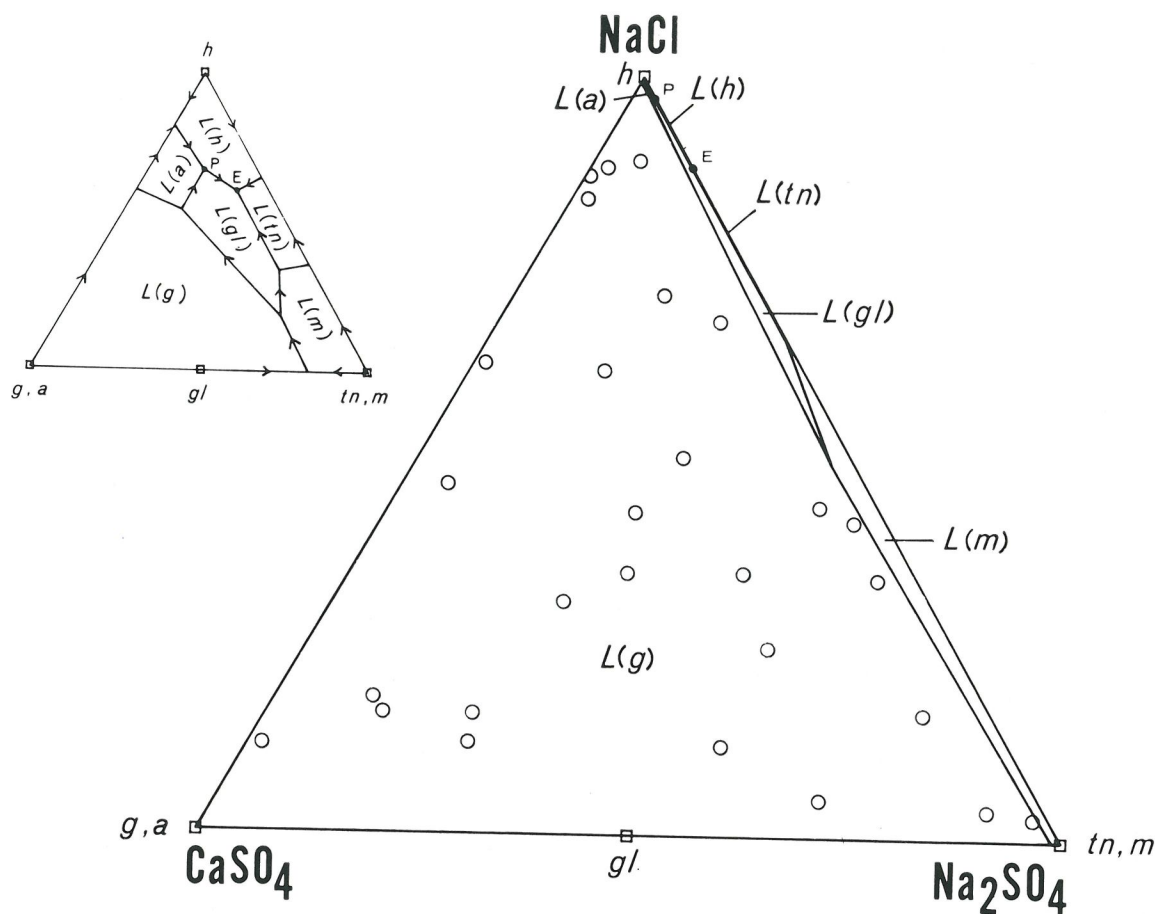


FIG. 10. Phase relations and compositions of brines in the system $\text{NaCl-CaSO}_4\text{-Na}_2\text{SO}_4\text{-H}_2\text{O}$. Phase boundaries at 25°C , calculated from D'Ans (1933). Symbols as in Figure 9, and g: gypsum, a: anhydrite, gl: glauberite. Insert is schematic to clarify the phase fields. The synthetic brines have been plotted at the moment of gypsum saturation, at which point their fate is fully defined. In mole percent.

Lake Magadi. A detailed study of the evolution of Lake Magadi, Kenya, brines is given elsewhere in this volume (Eugster, 1970). Figure 12 shows evaporation paths for four river waters of the Magadi basin: Endosapia, Oloibortoto and Uaso Nyiro (one near Magadi and the other at the entrance to Lake Natron). Magadi hot springs and brines are also plotted, as are the calculated brines formed by evaporation of four large East African lakes (Naivasha, Victoria, Tanganyika and Rudolf). All evaporation paths are very short and end well within the trona field, as, of course, they should. One major anomaly, however, is the exceedingly low sulfate content of the Magadi brines. This could be due either to analytical difficulties with respect to the sulfate determination in concentrated brines, to removal of sulfate by bacterial reduction, or to inflow waters much poorer in sulfate. A further possibility is the freezing out of mirabilite, which has been observed in Lake Magadi in small quantities (see Eugster, 1970).

Except for sulfate, the agreement between calculated and natural brines is excellent. It is clear why Magadi has precipitated so much trona, and is not yet saturated in halite.

This is not a peculiarity of the Magadi basin, but would be the fate of some of the largest fresh-water lakes of East Africa, such as Victoria, Tanganyika and Rudolf, if they were subjected to intense evaporation.

Deep Springs Lake. Jones (1965, 1966) has discussed in detail the hydrology, hydrochemistry and mineralogy of the Deep Springs playa. Direct inflow into the lake is provided primarily by three spring groups: Buckhorn Springs (BHS) in the Southeast, Corral Springs (CS 1 and CS 2) in the east and Bog-Mound Springs (NBS, WBS, CBS, EBS) in the north. The perennial rivers primarily responsible for ground water recharge are Birch Creek (BC), Wyman Creek (WC) and Crooked Creek (CC). Figure 13 shows the evaporation paths calculated for a few typical waters. The perennial creeks all yield Na-Cl-SO_4 (Group b) brines, as do the Buckhorn Springs and one of the Bog Mound Springs (NBS). These springs can be derived compositionally from the Wyman-Crooked Creek system by calcite precipitation and two-fold concentration, as is shown both in the anion and cation diagrams. BHI is a sample from an

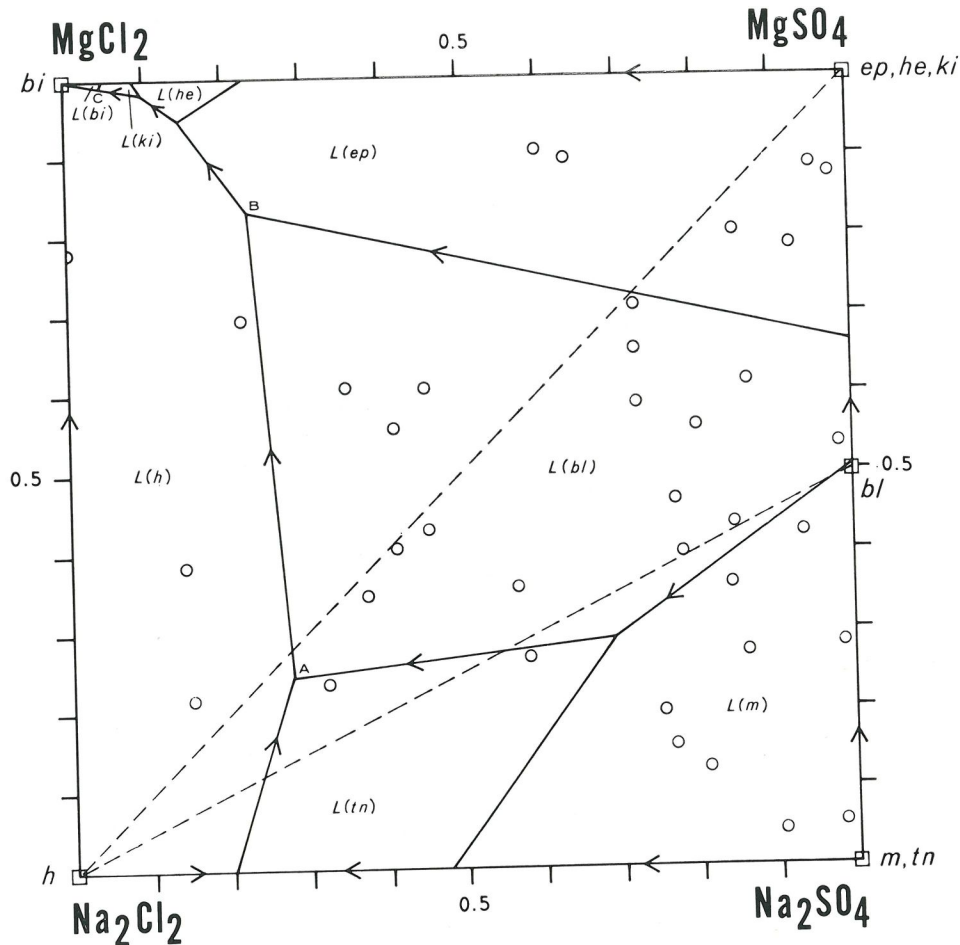


FIG. 11. Phase relations in the reciprocal system Na-Mg-SO₄-Cl at 25°C, based on the data of D'Ans (1933) and Autenrieth and Braune (1960). Symbols as in Figure 9 and bl: bloedite, ep: epsomite, he: hexahydrate, ki: kieserite, bi: bischofite. Brines plotted are those produced by paths II, IIA, III and IV in Figure 7 at ionic strengths of 5. In mole percent.

inflow channel between the Buckhorn springs and the lake, and it clearly relates to the springs through mirabilite precipitation. Birch Creek water is rich enough in sulfate to precipitate considerable amounts of gypsum but does not, presumably because of early mixing with the other springs poorer in sulfate and richer in sodium. The Corral Springs (especially CS 2) and Bog-Mound Springs (EBS, CBS, WBS) give mixed (Group a) brines. They must draw on sources other than the streams, a conclusion reached by Jones (1965) through hydrologic arguments. CSI is from an inflow channel below the Corral Springs. It cannot obtain its composition solely by evaporation of the Corral Spring water, but must have dissolved substantial amounts of efflorescent crusts consisting of halite and thenardite.

Figure 14 gives the comparison of the calculated with the natural brines. Immediately obvious is the connection between the sag pond and the Corral Springs. A mixture of CS 1 and CS 2, combined with evaporation and precipitation of calcite and sepiolite, yields the sag pond water at its high stage (low Cl values). This brine precipitates

mirabilite and trona and moves towards the composition of the low stage (high Cl values), at which time burkeite and trona precipitate.

The lake brines are a different matter. Their compositions correspond to synthetic brines derived from Buckhorn and N Bog-Mound Springs, with a small addition from the other sources. Evaporation leads to mirabilite precipitation, with corresponding enrichment in chloride. The surface brines have surprisingly constant carbonate + bicarbonate content, which is probably due to loss of CO₂ to the atmospheric reservoir. Intercrustal brines cluster near point P, representing the assemblage brine + thenardite + burkeite + halite. If we consider that final evaporation proceeds above 20°C, say at 25–30°C, the correspondence is better still, as shown by point P, drawn for brine + thenardite + burkeite + halite at 35°C. The sequence mirabilite (or thenardite) → burkeite → halite predicted for the Buckhorn Springs from Figure 14 is precisely the sequence observed by Jones (1965) for the horizontal zonation of the lake deposits and in the vertical sequence of the

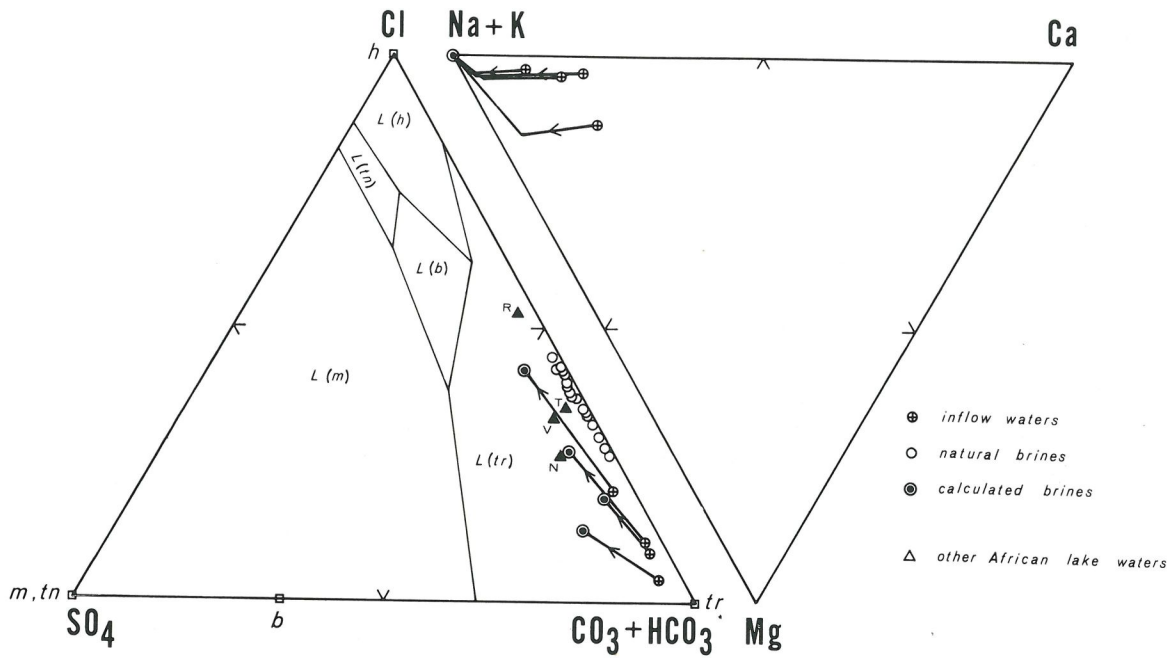


FIG. 12. Evaporation paths and natural brines from the Magadi area (data from Talling and Talling, 1965, and Eugster, 1970). Other dilute East-African lakes: N: Naivasha, V: Victoria, T: Tanganyika, R: Rudolf. Phase boundaries are from Figure 9. In mole percent.

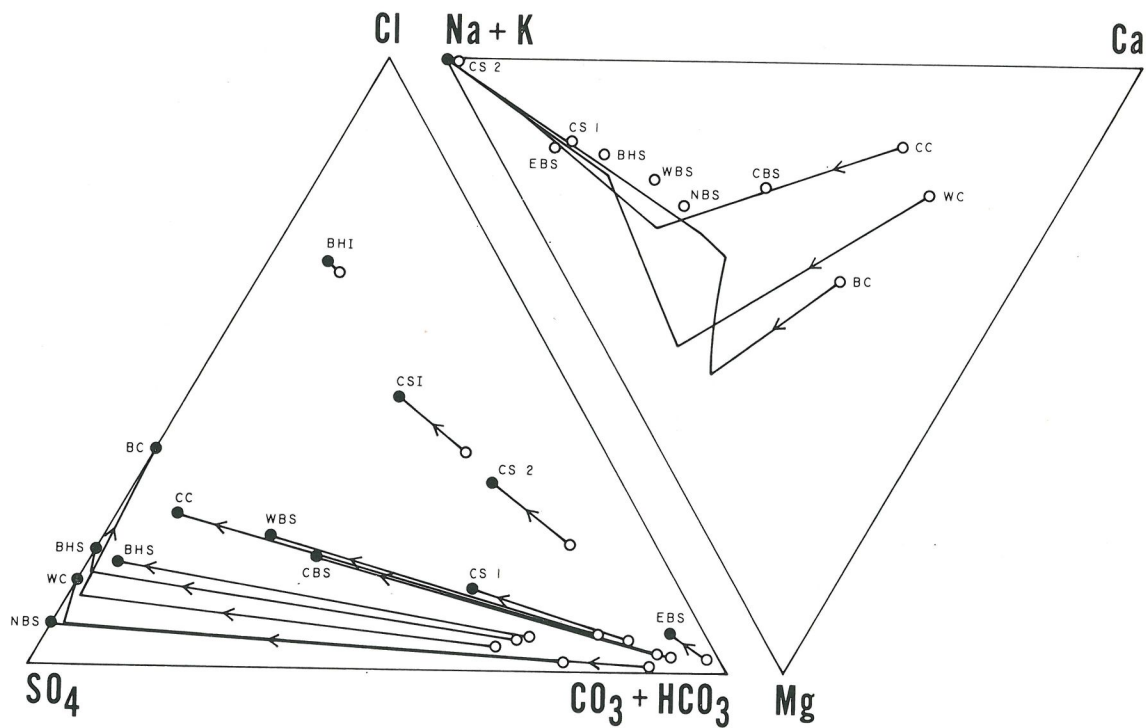


FIG. 13. Evaporation paths calculated from Deep Springs inflow waters. Analyses from Jones (1965). BC: Birch Creek; CC: Crooked Creek; WC: Wyman Creek; BHS: Buckhorn Springs; Bog-Mound Springs are NBS (north-west), WBS (west), CBS (central), EBS (eastern); CS 1 and CS 2 are Corral Springs 1 and 2, CSI is an inflow channel below CS 1 and CS 2 and BHI is an inflow channel below the Buckhorn Springs. The cation diagram shows paths for the creeks, and starting compositions only for springs. In mole percent.

salt crusts. Missing is the gaylussite zone, which occupies the area surrounding the thenardite zone. Gaylussite ($\text{Na}_2\text{CO}_3 \cdot \text{CaCO}_3 \cdot 5\text{H}_2\text{O}$) probably forms by reaction of calcite or dolomite with the alkaline lake brines, and therefore cannot be dealt with in our model.

Figure 14 demonstrates that our simple model is capable of explaining the compositions of brines and evaporites found at Deep Springs, if we accept the Buckhorn and NW Bog-Mound Springs as the dominant inflow. The contribution from the Corral Springs can be at most 20 percent of the total inflow. This is at variance with the estimated inflow rates for the major spring systems (Jones, 1965), but may simply emphasize the importance of seasonal flow variation. The intercrustal brines can be derived from the lake brines by precipitation of mirabilite, thenardite and burkeite. The burkeite production is lower than it would be in a closed system because of CO_2 loss to the atmosphere.

Saline Valley. The evaporite deposit of Saline Valley, California, has been discussed by Hardie (1968). Inflow to the playa is entirely subsurface and comes from three main source areas: (1) the perennial streams of Hunter, Beveridge and McElvoy Canyons and the Badwater and Mine Camp Springs along the western divide (Inyo Mountains), (2) the Grapevine Canyon stream system in the southeast, and (3) the group of hot springs (Upper, Palm, Lower Warm and Many Springs) in the northeast. Evaporation paths calculated for the best analyses of these waters are

shown in Figure 15. The hot springs yield $\text{Na}-\text{CO}_3-\text{SO}_4-\text{Cl}$ brines (Group a) while all the remaining waters, which are the main input to the playa, end in the system $\text{Na}-\text{Cl}-\text{SO}_4$ (Group b brines). This latter group of waters all precipitate gypsum at a concentration factor of about 16 times. The paths followed on further evaporation are shown in the phase diagram for the system $\text{CaSO}_4-\text{Na}_2\text{SO}_4-\text{NaCl}-\text{H}_2\text{O}$, Figure 16. This analysis confirms the previous findings (Hardie, 1968), but goes further and permits better resolution of the hydrology.

As can be seen from Figure 16, the Grapevine Canyon stream (GC, the main inflow from the south) would yield the evaporation sequence gypsum→gypsum+glauberite→glauberite→glauberite+halite→glauberite+halite+thenardite. This sequence was observed on the south side of the playa as concentric zones and the dilute brines from the gypsum zone of this area were shown to be the parent waters of this sequence (Hardie, 1968). The present analysis shows that these gypsum brines clearly can be derived only from the Grapevine Canyon waters. The main inflow from the west and northwest is represented in Figure 16 by Hunter (HC) and Beveridge (BC) Canyon streams. These waters should produce the sequence gypsum→gypsum+glauberite→gypsum+glauberite+halite. A pure glauberite zone was not found in the northwest sector of the playa but was inferred by analogy with the opposite side of the playa (Hardie, 1968). As Figure 16 shows, with Beveridge and Hunter Canyon streams as the parent waters

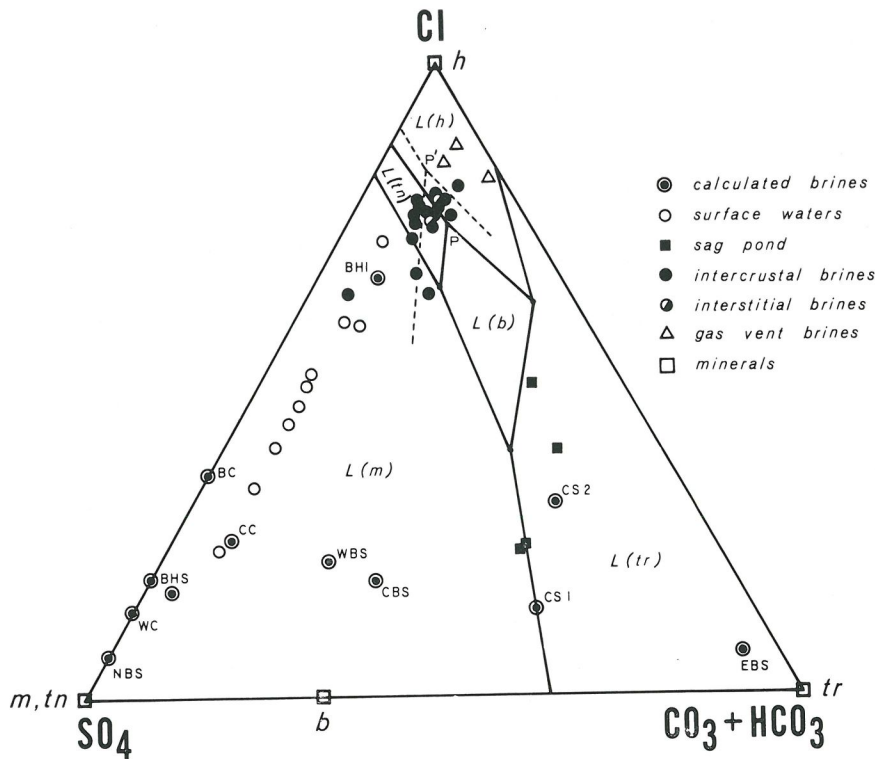


FIG. 14. Calculated and actual brines for Deep Springs. Abbreviations as in Figure 13 and Figure 9. Solid phase boundaries are from Figure 9 (20°C) and dashed curves are for 35°C in the vicinity of the "peritectic" point P. In mole percent.

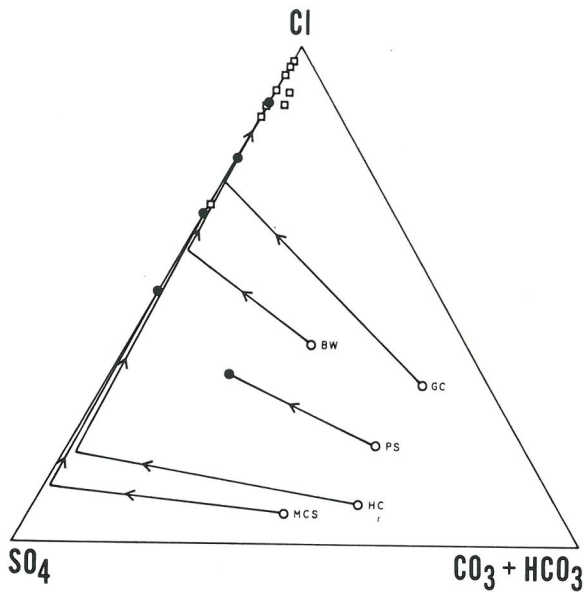


FIG. 15. Calculated evaporation paths for some natural waters inflow to Saline Valley, Calif. (data from Hardie, 1968). Open circles—initial waters equilibrated with atmospheric P_{CO_2} ; solid circles—calculated brine composition at $I \sim 5$; squares—natural brines. MCS—Mine Camp Spring, HC—Hunter Canyon stream, PS—Palm Spring, BW—Badwater springs, GC—Grapevine Canyon stream. In mole percent.

this glauberite zone should not, in fact, be present here. What should be looked for instead is a gypsum + glauberite + halite zone.

Evaporation of the northeast group of hot springs should produce a mixed brine (Figure 17) almost completely devoid of alkaline earths. Continued evaporation at 25°C should produce the assemblage thenardite + burkeite + halite. The only possible natural analogs, as suggested previously (Hardie, 1968, p. 1294), are the calcium-poor brines of the northeast corner of the playa (shown in Fig. 17 as squares). These brines, however, carry far too much chloride and too little carbonate. The co-existing salts were mirabilite + halite, and no burkeite was observed (Hardie, 1968, Table 1). When collected, the temperature of these brines was about 15°C , and, as is demonstrated in Figure 17, the compositions are perfectly consistent with the assemblage mirabilite + halite at 15°C . Thus the hot springs alone cannot be the parent waters for these low calcium brines. What is required is an inflow water that will show little increase in either Ca or $\text{CO}_3 + \text{HCO}_3$ on evaporation (a water with $\Delta = 0$). The composition of such a brine at the point of first precipitation of mirabilite will then lie almost on the SO_4 —Cl edge in Figure 17. Perhaps such a parent water could be obtained by subsurface mixing of hot spring inflow with the inflow from the northwest.

Other basins. Few closed basins have been studied in as much detail as Deep Springs, Magadi and Saline Valley. However, the evaporation model can provide some insight even where little data are available. To illustrate this point, Figure 18 presents two more basins, Great Salt Lake and Abert Lake, without, however, considering the details of their hydrology and chemistry. The data for Abert Lake are taken from Jones (1966) and those for

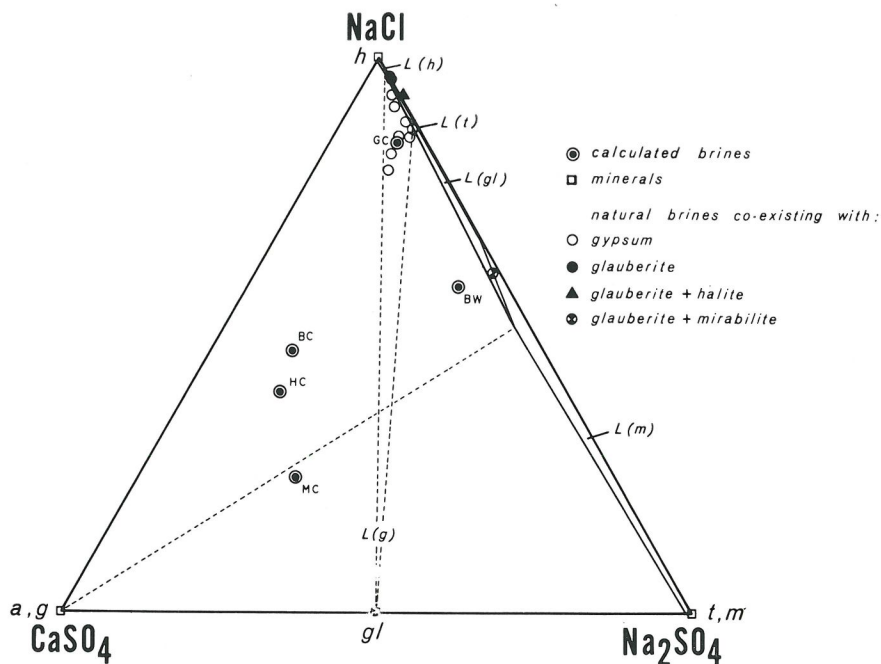


FIG. 16. Calculated and natural brines for Saline Valley in the system CaSO_4 - Na_2SO_4 - NaCl - H_2O (mole %). Field boundaries and symbols as for Figure 20. The calculated brine compositions (abbreviations as in Figure 15) are given at the point of first precipitation of gypsum.

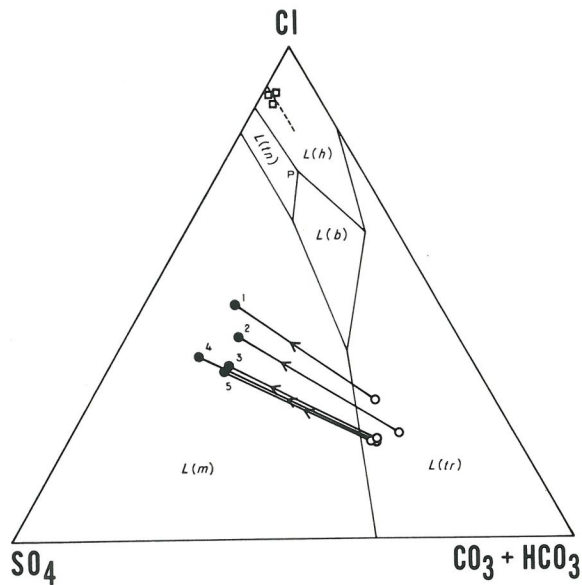


FIG. 17. Calculated and natural brines for Saline Valley in the system $\text{Na}_2\text{CO}_3\text{-NaHCO}_3\text{-Na}_2\text{SO}_4\text{-NaCl-H}_2\text{O}$ (mole %). Field boundaries and symbols as given in Figure 9. The short dashed line is the halite + mirabilite boundary at 15°C . Open circles—initial waters equilibrated with atmospheric P_{CO_2} ; solid circles—calculated brines at $I \sim 5$. Calculated evaporation paths join the initial and final waters. Squares are natural brines. 1—Many Springs, 2 and 3—Lower Warm Spring, 4 and 5—Palm Spring.

Great Salt Lake from Hahl and Langford (1964), White *et al.* (1963, composite of 126 samples) and Whitehead and Feth (1961). The data show very clearly that simple evaporation of Chewaucan River (CR 1 and CR 2) inflow cannot lead to the chloride enrichment necessary for the Abert Lake brines without massive trona and burkeite precipitation. The fact that one of the peripheral springs to Abert Lake (AS) fits the evaporative model much better indicates additional fractionation processes taking place at the lake margin (Jones and VanDenburgh, 1966). Abert Lake waters themselves lie fairly close to the trona-halite boundary for atmospheric P_{CO_2} ; and, indeed, these are the phases found in isolated ponds on peripheral mud flats.

The Bear (BR), Jordan (JR) and Weber (WR) rivers are the major inflow to Great Salt Lake and they would produce sodium sulfate-chloride brines through evaporation. As Figure 18 demonstrates, simulated evaporation of the waters of the Bear and Jordan rivers (which together provide almost 70 percent of the inflow, see Hahl and Langford, 1964, p. 14), closely reproduces the present lake brine anion compositions. The predicted solid precipitation sequence is calcite-sepiolite-gypsum-halite; mirabilite will appear only by winter freezing-out. A similar fate was calculated for the lake-shore springs and the drainage canal waters (not shown in Fig. 18). On the other hand, the Weber river (14% of the inflow) will produce brines far richer in sulfate than the reported natural brines, even after massive mirabilite-thenardite precipitation (Fig. 18). This indicates that the Weber river waters must mix with the other inflow waters before evaporation has proceeded too far.

CONCLUSIONS

The model we have presented here for the evolution of closed-basin brines is based on evaporative concentration in equilibrium with the atmosphere, coupled with fractional crystallization of calcite, sepiolite and gypsum. The model can handle any starting composition in terms of SiO_2 , Ca, Mg, Na, K, HCO_3 , CO_3 , SO_4 and Cl. We have not considered interaction of the brines with their precipitates and other solids. At high concentrations we have replaced calculations by standard graphical procedures, based on published brine equilibria.

In spite of its simplicity, the model provides some very real insights into the development of closed-basin brines. We have been able to duplicate the wide spectrum of natural brine compositions and to show that brine evolution is governed by a few crucial steps: the precipitation of calcite, a magnesium silicate and gypsum. Calcite precipitation always initiates these steps and causes the first fundamental division of brine compositional trends. It occurs very early, and at an ionic strength at which activities are still well known and ion pairs can be safely ignored. Of course, refinements to take account of ion association and $a_{\text{H}_2\text{O}}$ changes are desirable for higher concentrations, but they will not fundamentally alter the conclusions with respect to the origins of the brine composition diversity.

The model confirms the view of Jones (1966), Jones and VanDenburgh (1966) and Hardie (1968) that the compositional fate of a brine is already defined at the time it is a

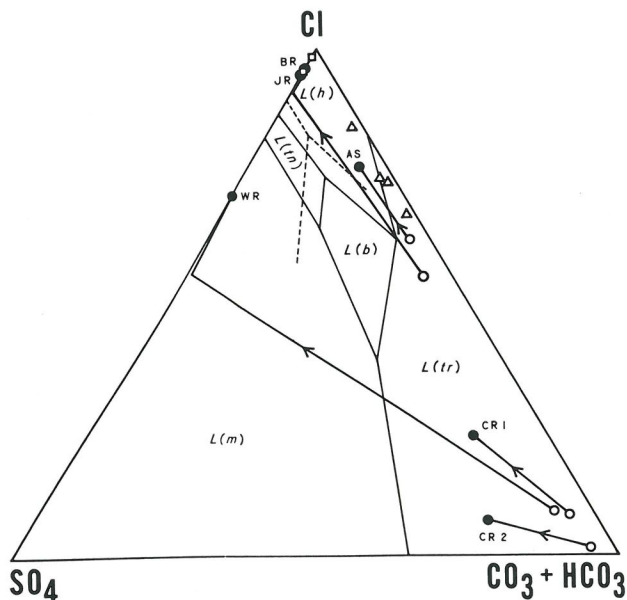


FIG. 18. Calculated evaporation paths and natural brines for Abert Lake, Oregon, and Great Salt Lake, Utah. Open circles—initial waters equilibrated with atmospheric P_{CO_2} ; solid circles—calculated brines at $I \sim 5$. CR 1 and 2; Chewaucan River. AS: Abert Lake Spring #2. Triangles: Abert Lake brines. BR: Bear River. JR: Jordan River. WR: Weber River. Open squares: Great Salt Lake brines. Calculated evaporation path for Jordan River water not shown. Solid phase boundaries are for 20°C (see Fig. 9) and dashed boundaries for 35°C (see Fig. 14). In mole percent.

dilute spring, river or lake water. This fate is inherited from the weathering reactions which are responsible for its initial composition. Therefore, the relation between lithology and brine composition is governed by the relation between dilute water composition and lithology. However, few generalizations can be made and each water must be considered individually.

Silica plays an important, and not yet fully understood role. This is indicated by the fact that certain very common natural brine types (group d) can only be simulated by suppressing sepiolite precipitation through using unreasonably low silica levels in the calculation. The type of silicate and kinetic factors are probably decisive. We know from many natural examples that only a very small fraction of the silica remains in the brine during evaporative concentration.

We have tested the usefulness of the model by applying it to some well-studied closed basins. The agreement between calculated and actual brines is generally good, testifying to the validity of the assumptions. In fact, the model evaporation has proved itself to be a powerful hydrologic tool, telling us which waters may be related to each other by simple evaporation and which may not. Every closed basin can be fruitfully subjected to this analysis, but, because the model is very general, each particular basin will demand its specific refinement.

To us perhaps the most persuasive argument for the value of the model is the fact that it uncovered a number of surprising aspects about those basins most familiar to us.

LIMITATIONS OF THE MODEL

The very real limitations of the model are obvious from our applications and conclusions. We would like to refer to problems connected with silica, alkalis, brine-solid interactions and compositional limitations.

The silica problem first became obvious when we were forced to keep silica artificially at a constant level and when we could derive the Na_2SO_4 — MgSO_4 brines only by suppressing SiO_2 . In fact, even the choice of sepiolite, in which we followed Garrels and Mackenzie (1967), is somewhat arbitrary, since sepiolite is not a common mineral. Perhaps more reasonable would be the formation of a Mg-montmorillonite at the expense of kaolinite. The eventual solution to the silica problem can only come from detailed studies of natural environments.

The model lumps K with Na, and hence does not affect the calculated Na/K ratio. Yet we know very well that this is not realistic for natural environments, where K is lost very rapidly during evaporation, presumably through ion exchange with clay minerals. Hence, closed-basin waters, unlike sea water, do not usually yield potassium-rich brines, presumably because of the small amount of brine in relation to the exchangeable material available.

Brine-solids interactions have not been considered by the model, and yet such interactions are known to be very common in natural situations throughout the whole concentration range. In the dilute stage, potassium and silica removal seem to be common. We have also mentioned the

formation of glauberite and gaylussite by reaction of brines with gypsum and calcite respectively. Among the most concentrated brines one often notices a chloride enrichment which can best be related to recycling of saline matter through differential solution. Efflorescent crusts can be very important in this respect. Organic activity, too, may significantly modify brine evolution, for instance through removal of sulfate by reduction to sulfide.

The compositional restrictions we have imposed on the model are not very serious, since they encompass the vast majority of closed basin brines. We have, however, specifically excluded from consideration boron-rich deposits such as Searles Lake, as well as nitrates, phosphates, fluorides and others. For deposits of this kind, the model clearly needs major modification.

The calculations are based on a constant P_{CO_2} of $10^{-3.5}$ atm. This is a reasonable assumption for most evaporative situations, but it need not always apply. For Magadi, for instance, (see Eugster, 1970), we had to stipulate subsurface evaporation and the springs seem to indicate a P_{CO_2} of $10^{-1.8}$. We have found that a change of this magnitude does not fundamentally alter the fate of a particular water, though it does, of course, affect the composition of the final brine.

Perhaps the most serious limitation of the approach presented here is not internal, but is connected with the quality of the water analyses available. Many water analyses are not electrically balanced, and they must be adjusted before they can be subjected to the calculations. The assignment of the errors often has a profound effect on the final composition, because of the multiplication with large evaporation factors. It is essential, therefore, to obtain analyses of the very highest quality.

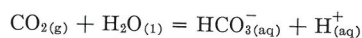
ACKNOWLEDGEMENTS

Dr. Blair F. Jones of the U. S. Geological Survey shares much of the credit due for this contribution. Throughout the ten years of our entanglement with nonmarine evaporites he has been an unselfish friend and colleague and a constant source of information, ideas and good cheer. We also thank J. R. Wood for help with computing problems.

This research was supported in part by National Science Foundation Grant #GA 1507 and Petroleum Research Fund Grant #2093 C.

APPENDIX

Derivation of the equations used in the computer program. For the reaction



we have

$$\begin{aligned} (K_a)_{P,T} &= a_{\text{HCO}_3^-} \cdot a_{\text{H}^+} / a_{\text{CO}_2} \cdot a_{\text{H}_2\text{O}} \\ &= 10^{-7.82(25^\circ\text{C}, 1 \text{ atm.})}^1 \end{aligned} \quad (1)$$

where

- (i) for the individual ions $a_i = m_i \gamma_i$ and $(a_i/m_i) \rightarrow 1$ as $m_i \rightarrow 0$.
- (ii) $a_{\text{CO}_2} = f_{\text{CO}_2} / f_{\text{CO}_2}^\circ \simeq P_{\text{CO}_2} / P_{\text{CO}_2}^\circ = |P_{\text{CO}_2}|$ for $P_{\text{CO}_2}^\circ = 1$
- (iii) $a_{\text{H}_2\text{O}} = f_{\text{H}_2\text{O}} / f_{\text{H}_2\text{O}}^\circ \simeq P_{\text{H}_2\text{O}} / P_{\text{H}_2\text{O}}^\circ$

where $P_{\text{H}_2\text{O}}^\circ$ is P of pure liquid H_2O at P (total) and T .

¹ Unless otherwise stated, values are taken (or calculated) from data of Garrels and Christ (1965).

if we assume very dilute solution ($a_{H_2O} \sim 1$) and atmospheric $P_{CO_2} = 10^{-3.5}$ atm., then we have from equation (1)

$$mHCO_3^- = 10^{-11.32}/\gamma HCO_3^- \cdot aH^+ \quad (2)$$

Similarly we can also show that under the same conditions

$$mCO_3^{2-} = 10^{-21.65}/\gamma CO_3^{2-} \cdot aH^{+2} \quad (3)$$

and

$$mOH^- = 10^{-14.0}/\gamma OH^- \cdot aH^+ \quad (4)$$

For a natural water (ignoring ion pairing) we have by electrical neutrality

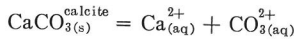
$$2mCO_3^{2-} + mHCO_3^- + mOH^- - mH^+ = 2mCa^{2+} + 2mMg^{2+} + mNa^+ + mK^+ - 2mSO_4^{2-} - mCl^-$$

If we assume atmospheric P_{CO_2} , $a_{H_2O} = 1$, $T = 25^\circ C$, $P(\text{total}) = 1$ atm., and if we neglect mH^+ (which is very small, $< 10^{-6}$), we get on substitution of the equations (2), (3) and (4):

$$\left(\frac{10^{-21.35}}{\gamma CO_3^{2-} \cdot aH^{+2}} \right) + \left(\frac{10^{-11.32}}{\gamma HCO_3^- \cdot aH^+} \right) + \left(\frac{10^{-14.0}}{\gamma OH^- \cdot aH^+} \right) = 2mCa^{2+} + 2mMg^{2+} + mNa^+ + mK^+ - 2mSO_4^{2-} - mCl^- \quad (5)$$

The right hand side of this expression is known from the chemical analysis and so the equation can be used to calculate the pH of any given natural water in equilibrium with atmospheric P_{CO_2} at $25^\circ C$, if we know the values of γ_i . These latter can be calculated from the Debye-Hückel equation. However, before we can compute γ_i , we need to know the ionic strength, $I = \frac{1}{2} \sum_i m_i z_i^2$. This in turn is dependent upon our knowing all the m_i 's, which in fact, we are trying to determine. The method of solution of this equation then must be one of successive approximations: (a) assume the initial values of m_i to get I and hence γ_i , (b) solve equation (5) for pH , (c) using this pH value recalculate m_i for the pH -dependent species using equations (2), (3) and (4), (d) re-solve equation (5) using these new values of m_i , (e) repeat the cycle until pH does not change.

Consider now this same CO_2 -equilibrated water in equilibrium with calcite. For the reaction



we have

$$(K_a)_{P,T} = aCa^{2+} \cdot aCO_3^{2-} / aCaCO_3 = 10^{-8.34}(25^\circ C, 1 \text{ atm.}) \quad (6)$$

If the calcite is pure $CaCO_3$ (that is, in its standard state for which $aCaCO_3 = 1$) then we get by combining (6) and (3):

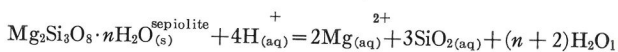
$$mCa^{2+} = 10^{13.31} \cdot aH^{+2} / \gamma Ca^{2+} \quad (7)$$

Now calcium is a pH -dependent species and the electrical neutrality equation can be written as:

$$\left(\frac{10^{-21.35}}{\gamma CO_3^{2-} \cdot aH^{+2}} \right) + \left(\frac{10^{-11.32}}{\gamma HCO_3^- \cdot aH^+} \right) + \left(\frac{10^{-14.0}}{\gamma OH^- \cdot aH^+} \right) - \left(\frac{10^{13.61} \cdot aH^{+2}}{\gamma Ca^{2+}} \right) = 2mMg^{2+} + mNa^+ + mK^+ - 2mSO_4^{2-} - mCl^-$$

This expression can be solved by the iteration method we used for equation (5) to give the pH of a water in equilibrium with calcite and atmospheric P_{CO_2} .

At saturation with sepiolite we have,



and

$$(K_a)_{P,T} = (aMg^{2+})^2 (aSiO_2)^3 (aH_2O)^{n+2} / (aMg_2Si_3O_8 \cdot nH_2O) (aH^+)^4 = 10^{18.8}(25^\circ C, 1 \text{ atm.}) \quad (\text{Wollast } et \text{ al., } 1968)$$

Then, for pure stoichiometric sepiolite (unit activity)

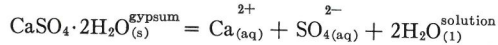
$$mMg^{2+} = 10^{9.4} (aH^+)^2 / (aSiO_2)^{3/2} \gamma Mg^{2+}$$

Substituting this into equation (5) gives

$$\left(\frac{10^{-21.35}}{\gamma CO_3^{2-} \cdot aH^{+2}} \right) + \left(\frac{10^{-11.32}}{\gamma HCO_3^- \cdot aH^+} \right) + \left(\frac{10^{-14.0}}{\gamma OH^- \cdot aH^+} \right) - \left(\frac{10^{9.7} \cdot aH^{+2}}{aSiO_2^{3/2} \cdot \gamma Mg^{2+}} \right) = 2(mCa^{2+}) + mNa^+ + mK^+ - 2(mSO_4^{2-}) - mCl^-$$

This is the sepiolite equilibrium.

The method cannot handle gypsum alone but if calcite and gypsum co-precipitate then both calcium and sulfate can be expressed in terms of pH . For gypsum equilibrium we have,



and

$$(K_a)_{P,T} = aCa^{2+} \cdot aSO_4^{2-} \cdot aH_2O^2 / aCaSO_4 \cdot 2H_2O = 10^{-4.4}(25^\circ C, 1 \text{ atm.}) \quad (\text{Marshall and Slusher, } 1966)$$

For pure gypsum (unit activity) and $a_{H_2O} = 1$

$$mSO_4^{2-} = 10^{-4.4} / aCa^{2+} \cdot \gamma SO_4^{2-}$$

but because of the coexisting calcite, equation (7) must also hold, then

$$mSO_4^{2-} = 10^{-17.71} / \gamma SO_4^{2-} \cdot aH^{+2}$$

For the coexistence of calcite and gypsum we get then,

$$\left(\frac{10^{-21.35}}{\gamma CO_3^{2-} \cdot aH^{+2}} \right) + \left(\frac{10^{-11.32}}{\gamma HCO_3^- \cdot aH^+} \right) + \left(\frac{10^{-14.0}}{\gamma OH^- \cdot aH^+} \right) - \left(\frac{10^{13.61} \cdot aH^{+2}}{\gamma Ca^{2+}} \right) + \left(\frac{10^{-17.41}}{\gamma SO_4^{2-} \cdot aH^{+2}} \right) = 2mMg^{2+} + mNa^+ + mK^+ - mCl^-$$

In a similar manner we produce for the co-existence of calcite and sepiolite:

$$\left(\frac{10^{-21.35}}{\gamma CO_3^{2-} \cdot aH^{+2}} \right) + \left(\frac{10^{-11.32}}{\gamma HCO_3^- \cdot aH^+} \right) + \left(\frac{10^{-14.0}}{\gamma OH^- \cdot aH^+} \right) - \left(\frac{10^{13.61} \cdot aH^{+2}}{\gamma Ca^{2+}} \right) - \left(\frac{10^{9.7} \cdot aH^{+2}}{\gamma Mg^{2+} \cdot aSiO_2^{3/2}} \right) = mNa^+ + mK^+ - 2mSO_4^{2-} - mCl^-$$

and for calcite+sepiolite+gypsum:

$$\left(\frac{10^{-21.35}}{\gamma CO_3^{2-} \cdot aH^{+2}} \right) + \left(\frac{10^{-11.32}}{\gamma HCO_3^- \cdot aH^+} \right) + \left(\frac{10^{-14.0}}{\gamma OH^- \cdot aH^+} \right) - \left(\frac{10^{13.61} \cdot aH^{+2}}{\gamma Ca^{2+}} \right) - \left(\frac{10^{9.7} \cdot aH^{+2}}{\gamma Mg^{2+} \cdot aSiO_2^{3/2}} \right) + \left(\frac{10^{-17.41}}{\gamma SO_4^{2-} \cdot aH^{+2}} \right) = mNa^+ + mK^+ - mCl^-$$

REFERENCES

- D'ANS, J. (1933) *Die Lösungsgleichgewichte der Systeme der Salze Ozeanischer Salzablagerungen*. Kali-Forschungsanstalt, Berlin, 254 p.
- AUTENRIETH, H., AND G. BRAUNE (1960) Die Lösungsgleichgewichte des reziproken Salzpaars $\text{Na}_2\text{Cl}_2 + \text{MgSO}_4 + \text{H}_2\text{O}$ bei Sättigung an NaCl unter besonderer Berücksichtigung des metastabilen Bereichs. *Kali Steinsalz* **3**, 15-30.
- BRADLEY, W. H., AND H. P. EUGSTER (1969) Geochemistry and paleolimnology of the trona deposits and associated authigenic minerals of the Green River Formation of Wyoming. *U. S. Geol. Surv. Prof. Pap.* **496B**, 71 p.
- CLARKE, F. W. (1924) The data of geochemistry, 5th ed. *U. S. Geol. Surv. Bull.* **770**, 841 p.
- EARDLEY, A. J. (1938) Sediments of Great Salt Lake, Utah. *Amer. Ass. Petroleum Geol. Bull.* **22**, 1305-1411.
- EUGSTER, H. P. (1965) Sodium carbonate-bicarbonate minerals as indicators of P_{CO_2} . *J. Geophys. Res.* **71**, 3369-3377.
- (1970) Chemistry and origin of the brines of Lake Magadi, Kenya. *Mineral Soc. Amer. Spec. Pap.* **3**, 215-235.
- FETH, J. H., C. E. ROBERSON, AND W. L. POLZER (1964) Sources of mineral constituents in water from granitic rocks, Sierra Nevada, California and Nevada. *U. S. Geol. Surv. Water Supply Pap.* **1535-I**.
- GARRELS, R. M., AND C. L. CHRIST (1965) *Solutions, Minerals and Equilibria*. Harper and Row, New York, 450 p.
- , AND F. T. MACKENZIE (1967) Origin of the chemical composition of some springs and lakes. In *Equilibrium Concepts in Natural Water Systems*. American Chemical Society, Washington, D. C., p. 222-242.
- HAHL, D. C., AND R. H. LANGFORD (1964) Dissolved-mineral inflow to Great Salt Lake and chemical characteristics of the Salt Lake brine; Part II. *Utah Geol. Mineral. Surv., Water Resour. Bull.* **3**, 40 p.
- HARDIE, L. A. (1968) The origin of the Recent non-marine evaporite deposit of Saline Valley, Inyo County, California. *Geochim. Cosmochim. Acta* **32**, 1279-1301.
- HELGESON, H. C., R. M. GARRELS, AND F. T. MACKENZIE (1969) Evaluation of irreversible reactions in geochemical processes involving minerals and aqueous solutions—II. Applications. *Geochim. Cosmochim. Acta* **33**, 455-481.
- HUTCHINSON, G. E. (1957) *A treatise on Limnology, Vol. 1*. John Wiley and Sons, New York, 1015 p.
- JONES, B. F. (1965) The hydrology and mineralogy of Deep Springs Lake. *U. S. Geol. Surv. Prof. Pap.* **502-A**, 56 p.
- (1966) Geochemical evolution of closed basin waters in the western Great Basin. *Symp. Salt, 2nd Ohio Geol. Soc., Cleveland, Ohio*, **1**, 181-200.
- , AND A. S. VANDENBURGH, (1966) Geochemical influences on the chemical character of closed lakes. *Int. Ass. Sci. Hydrol. Publ.* **70**, 435-446.
- , S. F. RETTIG, AND H. P. EUGSTER (1967) Silica in alkaline brines. *Science* **158**, 1310-1314.
- LIVINGSTONE, D. A. (1963) Chemical composition of rivers and lakes. Data of Geochemistry, *U. S. Geol. Surv. Prof. Pap.* **440G**, 64 p.
- MAKAROV, S. Z., AND B. P. BLIDDEN (1938) Polytherms of the quaternary system $\text{Na}_2\text{CO}_3\text{-Na}_2\text{SO}_4\text{-NaCl-H}_2\text{O}$ and solid solutions of the burkeite type. *Izv. Akad. Nauk. SSSR* **10**, 866-892.
- MARSHALL, W. L., AND R. SLUSHER (1966) Thermodynamics of calcium sulfate dihydrate in aqueous sodium chloride solutions, 0-110°. *J. Phys. Chem.* **70**, 4015-4027.
- TALLING, J. F., AND I. B. TALLING (1965) The chemical composition of African lake waters. *Int. Rev. Ges. Hydrobiol.* **50**, 421-463.
- TEEPLE, J. E. (1929) Industrial development of Searles Lake brines. *Amer. Chem. Soc. Mono.* **49**, 182 p.
- WHITE, D. E., J. D. HEM AND G. A. WARING (1963) Chemical Composition of Subsurface Waters. *U. S. Geol. Surv. Prof. Pap.* **440-L**, 67p.
- WHITEHEAD, H. C., AND J. H. FETH (1961) Recent chemical analyses of waters from several closed basin lakes and their tributaries in the western United States. *Geol. Soc. Amer. Bull.* **72**, 1421-1426.
- WOLLAST, R., F. T. MACKENZIE, AND O. P. BRICKER (1968) Experimental precipitation and genesis of sepiolite at earth-surface conditions. *Amer. Mineral.* **53**, 1645-1662.